Physics – Uspekhi **37** (10) 961 – 990 (1994)

PACS numbers: 87.22.–q, 89.70.+c

From the dynamics of population autowaves generated by living cells to neuroinformatics

G R Ivanitskii¶, A B Medvinskii¶, M A Tsyganov

Contents

1. Introduction and statement of the problem **961**
1.1 Computer program and intellect; 1.2 Taxis, motility, reproduction; 1.3 Memory; 1.4 Autowaves
2. Population autowaves as a cooperative response of chemotactic bacterial cells **968**
2.1 Phenomenological model; 2.2 Zavalskii's theory; 2.3 Rivero's theory
3. Interaction between bacterial population waves and formation of static spatial structures **971**
3.1 Ω and KΩ structures; 3.2 TW waves
4. Unstable propagation regimes of population waves formed by motile chemotactic cells **979**
4.1 Stability of classical autowaves formed by elements devoid of memory; 4.2 Spontaneous bursting of the symmetry of population autowaves formed by mobile microorganisms possessing chemotaxis; 4.3 Instability of population autowaves generated by chemotactic cells
5. Synopsis **986**
References **988**

Abstract. Research into living cells and their communities can be extended to more general problems, e.g. what is the algorithm of data processing in living systems, or what is the difference between living systems and computers. It has been shown that a computerised system simulating cell behaviour, i.e. multiplication, motility, memory, and taxis, can be better at image processing than video-based automatic devices. Study of the dynamics of population waves formed by living cells is of special interest for autowave physics since population waves differ essentially from the 'classical' waves in active media. Mathematical models of population waves are found to feature an additional term describing not a chaotic but a directed motion of individual cells ('the effect of chemotaxis'). Detailed analysis of models like these and related phenomena (e.g. pattern formation as a result of population wave interaction, or symmetry bursting of population wave patterns) should be the subject of further research.

¶These authors' names are sometimes spelt Ivanitsky and Medvinsky in Western literature.

G R Ivanitskii, A B Medvinskii, M A Tsyganov Institute for Theoretical and Experimental Biophysics, Russian Academy of Sciences
142292 Pushchino, Moscow Region
Tel. (7-095) 925 5984; (7-095) 923 9668 (add. number 259)
E-mail: ivanitsky@venus.iteb.serpukhov.su

Received 26 May 1994
Uspekhi Fizicheskikh Nauk **164** (10) 000 – 000 (1994)
Submitted in English by the authors; edited by A Gelbtuch

1. Introduction and statement of the problem

1.1 Computer program and intellect

The aim of this paper is to review studies on the dynamics of population autowaves formed by living cells and of the structures generated by these autowaves.

We consider live cells and their populations as an object of research, an important tool whereby some general problems can be solved, such as: which algorithms do living systems employ to process information? What is the difference between live 'computers' and their man-made 'analogs' at the current stage of information technology?

Towards the middle of this century, scientific journals and journals popularising science started to feature papers under such headings as ''Brain as a calculating machine'', ''Are there thinking machines?'', ''Computer and human mind'', etc. No effort was spared in an attempt to design machines operating on the same principles as human brain and capable of reproducing and explaining its function.

What is the crux of the matter? The duration of a nerve impulse in a human brain is around 3 ms, and it is followed by a refractory 'tail' which is approximately twice as long. Therefore, human brain as a 'neuronal calculating device' can perform at a rate of not more than 10^2 operations per second whereas the operating speed of up-to-date microprocessors exceeds 10^7 s^{-1}. Computers which will shortly become available are expected to operate at 10^9 s^{-1} and it is predicted that their performance will be further raised to 10^{12} operations s^{-1} at the beginning of the next century.

Paradoxically, the 'low-performance' human brain is able to distinguish, in a fraction of a second, a cat from a dog, to recognise a familiar face in a crowd, and identify any letter in different handwritings or printed in different fonts, whereas 'high-speed' computers (even those with parallel logic) encounter great difficulties in solving prim-

itive recognition problems. This means that the brain is capable of doing 'something' extra which so far remains unexplained [1].

Advocates of the idea of artificial intelligence argue that computers deal with models (i.e. programs) rather than with natural phenomena. One such model may describe different phenomena. In this sense, programs are universal tools and can be expected to simulate adequately brain processes. From this viewpoint, all current constraints are due to simplifications which at present cannot be avoided and will be eliminated with the development of improved programs that will bring in qualitative changes in the intellectual capacities of computers. The degree of perfection of a program is assessed on the basis of experimental results obtained with the use of an operational approach the essence of which was outlined by Ashby [2]: (1) the method must be specified as a working tool, (2) it must be suitable for the evaluation of all sorts of material 'machines', both animate and inanimate, (3) the mode of information retrieval must be reproducible and readily demonstrable, (4) the 'machine' must be the sole source of information, the use of any other source being illegal.

Following this line of reasoning forty years ago, Turing [3] suggested a test designed to answer the question: ''Does the machine have intelligence?'' According to this method, the examiner offers two identically typed messages, one to a man and the other to a computer programmed to 'sensibly' answer questions. The program passes the test and the machine is judged to be intelligent if the examiner finds it impossible to differentiate between answers given by man and computer during a sufficiently long experimental period. The inadequacy of Turing's approach has recently been demonstrated by J Searle, an American philosopher, who suggested the so-called 'Chinese room' test [4]. Here, the observer presents a story and a few pertinent questions to a person in a sealed room. The story and the questions are written in Chinese, that is in hieroglyphs. The person in the sealed room has been previously instructed how to use hieroglyphs and can therefore operate with them guided by combinatorial rules although he does not know Chinese and the meaning of the messages remains incomprehensible to him. The observer knowing both spoken and written Chinese has the impression that the man in the room has the same faculties and can reasonably understand and answer questions. This test demonstrates that the semblance of reason can be achieved even if the meaning of the text evidently remains beyond understanding, being presented in an unintelligible form. For this reason, the ability of a technical device to operate with combinatorial rules (i.e. a program, even a most sophisticated one) does not necessarily prove its power of abstract thought. Moreover, Searle emphasises that detaching the program from the material from which the device is made is an unsubstantiated and artificial operation. The program and its material carrier must not be separated from each other because the real world does not develop through evolution of symbols and information signals from which computer programs are constructed. It is the long evolution of live organic systems which is responsible for their ability to think. That is why no analytic system based on or composed of a different material substrate and showing other types of innate responses may be considered intelligent [4].

This discussion may appear to have no sense because it needs to operate with such vague notions as 'mind' and 'intelligence', no matter how useful they might be for other purposes. It is, however, essential that the most important differences of opinion have a direct bearing on general problems of cognition. Many scientists thought it possible to make up a stock of axioms and rules in order to devise a model of the universe using computers and methods of formal logic to construct it stage by stage, in the way employed to prove theorems in mathematics. However, such an approach turned out to be in conflict with Godel's theorem which states that in a closed noncontradictory system based on postulates of formal logic there is always a likelihood of obtaining inferences which it is impossible to judge as true or false in the framework of a given system [5, 6]. This uncertainty may be referred to as 'the curse of indeterminate boundaries'. Another curse arises from the complexity of the problems to be solved and of the sorting procedure. What is 'complexity'? Kolmogorov [7, 8] proposed to use the size of the program (l) which transforms a given sequence $\{y_j\}$ to $\{x_i\}$ (in bits) as a measure of complexity of a given sequence of zeros and ones $\{x_i\}$ (such sequences may be used to describe any process). If the problem is not too complex, l is significantly less than the length N of sequence $\{x_i\}$ which can in this case be regarded as determinate. Otherwise, the process is not amenable to algorithmic reduction and can be regarded as irregular or random. For such processes, $l \sim N$ and the algorithm of transformation $\{x_i\} \rightarrow \{y_j\}$ is reduced to symbol-by-symbol presentation of the sequence $\{x_i\}$. Therefore, solution of problems associated with random processes is possible only if their spatial and temporal characteristics are available. Intermediate between completely irregular and completely regular problems amenable to algorithmic transformation, there is a class of problems with latent regularity [9]. These problems can be arbitrarily referred to as determinately-stochastic or stochastically-determinate. Transition from order to chaos progresses via such problems [10].

What ways and means can be used to solve problems with latent regularity, not to mention completely irregular problems? The traditional approach is based on a very simple idea. Consider a computer having $\mathfrak{N}$ stable states placed in an environment with latent regularity and $\mathfrak{M}$ stable states ($\mathfrak{N} > \mathfrak{M}$). Make the computer learn, that is make a set of $\mathfrak{N}$ stable states assume an index from a set of $\mathfrak{M}$ environmental states. This results in a computer model of the environment. In other words, the computer has managed to find latent regularity in a random process. This approach is currently employed in an attempt to construct computing devices that operate on the neural network principle [11, 12]. However, such an approach entails difficulties pertaining to the 'curse of indeterminate boundaries' and 'the curse of sorting'. According to a mathematical postulate, there is a self-contained ideal world of algorithms totally independent of human world. The objective is to understand the laws governing the former taking into account that interaction between man and real world is far from being ideal. In nature, the relationships between the object and its environment are reciprocal in that the object does not only depend on the environment but can also markedly change it. In other words, the calculation process affects the state of both the computer and the environment. Only low-speed computation capable of solving relatively simple problems allows an

arbitrary boderline between the object and the environment to be drawn.

Electronic data aquisition and processing entail absorption of energy from the environment and its re-emission in a different range both inside and outside the computing device. Data processing itself requires energy drawn from the outside. This energy is then released back in another form to the environment, changing its state. The question naturally arises: where is the boderline between the computer and the environment?

The 'noise' produced by a high-quality computer is negligibly low and in an adiabatically isolated system amounts to kT (where k is Boltzmann's constant and T is temperature) per one degree of freedom, i.e. $\sim 10^{-16}$ erg K^{-1}. However, even this small value assumes great importance when the number of degrees of freedom is large. Suppose that a machine with parallel logic sorts out possible states at a rate of 10^{22} s^{-1}. In this case the power emitted by even the most sophisticated machine would be around 100 kW and would have a serious effect on the environment.

Also, it should be borne in mind that biochemical 'computers' (e.g. biochips) release chemical products of their metabolic activity into the environment which makes the borderline between the organism and its surroundings obscure.

Moreover, it is necessary to know the parameters of the medium if its boundaries are to be determined. Construction of an 'intelligent machine' becomes a purely technological matter if the characteristics of the environment are available. Having determined the properties of the environ-ment, we have its description and hence the algorithm describing its behaviour. This algorithm can be loaded into the computer. Conversely, boundaries of the environment cannot be determined without the knowledge of its properties. It follows from this reasoning that there can be no universal algorithm for the purpose of discrimination. Nor is it possible to design a universal machine capable of differentiating situations regardless of their specific features. Finally, there is 'the curse of sorting'. If the computer has only 10^3 elements, it will have to sort out approximately 10^3 (!) states, which is actually impossible. At the same time, living systems are known to be highly efficient in solving complicated problems including those of image discrimination. Wherewith?

1.2 Taxis, motility, reproduction

Today, builders of artificial intelligence are putting their faith in physiological and psychological studies of human brain as a system adapted to solve problems arising from random processes with latent regularity. However, it is not so easy to identify essential parameters of brain function. Moreover, brain is so sensitive and functions as such a powerful amplifier of signals acting on it that it is hardly possible to establish physical threshold values below which signals cannot alter the state of the brain. Finally, there are so many feedback loops within the brain that it is almost impossible to study this organ on any other basis than considering it to be an integrated structure. However, such an approach is not very productive in terms of new constructive ideas for designing technological systems of artificial intelligence [1].

It occurred to us that, in order to devise approaches to the construction of a new class of machines with artificial intelligence, we should solve the problem of synchronous development of automaton structure and continuous broadening of its capacity rather than the problem of discrimination. We thought that instead of the relationship $\mathfrak{M} \rightarrow \mathfrak{N}$ referred to earlier, we should find a variant of automaton's behaviour in which the rate of increase in the number of stable states would be related to the rate of environmental changes. In this case, all the aforementioned 'curses' would be eliminated since filling of sets and location of their boundaries become immaterial. What matters is their dynamics.

Therefore, what we call 'intelligence' in the context of complex systems (bioorganisms including man) is a function of the development of both the systems and their environment. In other words, we have to study implementation of the inherent program of automaton development in a variable environment. It is assumed that the development of automaton structure will reflect development of the environment.

The analogous problem in biology is the study of morphogenesis (formation and development of live spatial structures). Paradoxically, we propose to look for a clue to the underlying mechanisms of rational behaviour by examining the behaviour of relatively simple microorganisms, e.g. by investigating changes in the behaviour of bacterial communities under variable environmental conditions [13]. A similar approach has been proposed by Japanese authors who, unlike ourselves, chose to study nematode populations *Caenorhabditis elegans* instead of bacterial communities [14]. What are the advantages of this approach? Before considering this question, it is necessary to review available data on the behaviour of bacterial cells including their motility, taxis, and reproduction.

Towards the end of the 19th century, Kohn, Engelman, and Pfeffer demonstrated the ability of certain bacteria cultured in a nutrient medium to change direction of their motion in search of a more favourable environment, in order to avoid adverse conditions [15–19]. Although systematic studies of bacterial cell motility and behaviour (including manifestations of bacterial memory) have a relatively short history, considerable progress has been made in this field during the last 25 years.

How do bacteria travel in space? A characteristic trait in many bacterial species is the use of specialised locomotor organelles, flagella. In peritrichous bacteria, flagella are randomly distributed over the surface of the body (*Escherichia coli, Salmonella typhimurium, Bacillus*, etc.; Fig. 1). Such cells are able to actively migrate, interrupting periods of oriented smooth swimming (free walk) by episodes of so-called tumbling. During periods of smooth

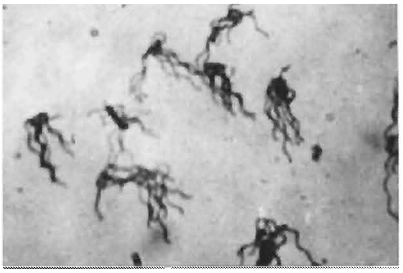

Figure 1. Bacteria *S. typhimurium* in the state of smooth swimming [20].

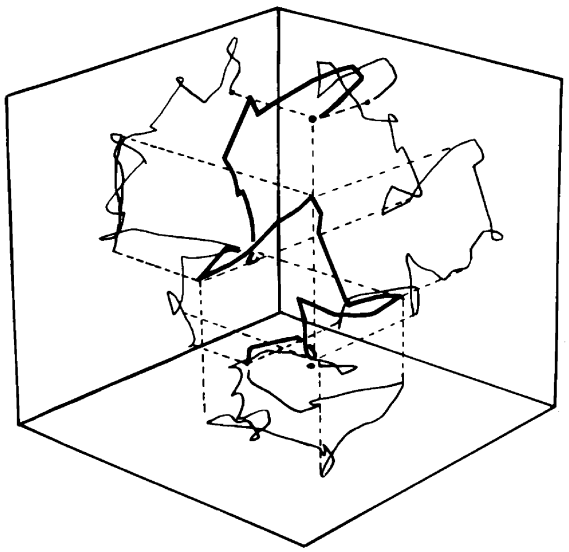

Figure 2. Random travel pattern of *E. coli* [25].

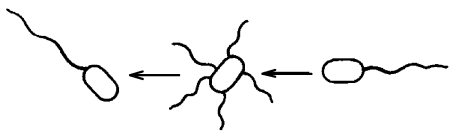

Figure 3. Altered direction of bacterial motion as a result of tumbling caused by untwining of the filament bundle [26].

swimming, flagella are rotated and converted into a concertedly operating helical bundle behind the cell body (Fig. 1). This generates a periodic force pushing the cell forward [21, 22]. Flagella rotated in the opposite sense cause the cell to lose orientation and travel through the environment by abrupt chaotic movements reminiscent of vibration and tumbling. Duration of a smooth swimming episode is normally 1 to 4 s whereas a tumbling episode lasts around 0.1 s [21, 23, 24] (Fig. 2). Tumbling frequency remains unaltered under constant environmental conditions. Each tumbling episode is followed by reorientation of the cell's motion [13, 21, 23, 25] (Fig. 3).

However, both tumbling frequency and smooth swimming intervals undergo changes where certain types of gradients are present in the media. If a bacterial cell happens to swim towards a more favourable environment (substrates producing such environment are termed attractants), the tumbling frequency decreases. Under unfavourable conditions (induced by the presence of so-called repellents), cells show an opposite response [23, 27–29]. Changing the tumbling frequency and walking randomly through its environ-ment, the cell gradually travels in the direction of increasing concentration gradient of the attractant or decreasing concentration gradient of the repellent (chemotaxis effects).

Generally speaking, taxis—the reaction to external stimuli—is a primeval feature of all living systems. For example, positive phototaxis accounts for the orientation of a bee or a sunflower towards the sun, whereas negative phototaxis (avoidance of light) is inherent in bugs and cockroaches. Stereotype response to external stimuli is a common trait in lower organisms, insects, reptiles, many bird species, and even in certain cell types of higher organisms. In mammals, including man, behaviour is not solely a function of instinct (imitating, play, sex, migratory, gregarious) but depends also on learning and is controlled by consciousness (upper cerebral cortex).

Oxygen, *N*-acetyl-D-glucosamine, D-galactose, D-glucose, L-aspartate, L-serine, and some other compounds act as attractants for *Escherichia coli* [13, 30–35] whereas fatty acids, alcohols, hydrophobic aminoacids as well as many other substances act as repellents [30, 35, 36].

Along with chemical substances, physical factors can also act as attractants or repellents. They include light [30, 37–42], temperature [30, 43–47], electric and magnetic fields [48–50], and gravitation [30, 51–56]. For instance, intense blue light can induce continuous tumbling in *E. coli*. This effect is thought to be related to flavin decomposition accompanied by oxidation of certain hypothetical chemical compounds that supposedly control bacterial behaviour [37–39, 57, 58]. Other examples are stimulation of *E. coli* motility by alternating electric fields and their inhibitory effect (ca. 70%) on chemotactic responsiveness of these bacteria [50].

An important factor is that all effects associated with the action of attractants and repellents occur not only in spatial gradients but also in temporal ones, i.e. bacteria respond to time-dependent changes in concentration of these compounds [27, 28]. This means that bacteria have memory.

In 1969, it was demonstrated that bacterial response to attractants is mediated through chemoreceptors [31]. Receptors are protein molecules capable of 'measuring' the concentration of certain compounds and conveying this information to the bacterial motor. In this way receptors are involved in modulation of the tumbling frequency [21, 30, 35, 40, 59–61].

The mechanism of bacterial chemoreception has not yet been fully explained. However, receptors have been shown to penetrate the cell membrane [26]. The outer portion of the receptor molecule binds attractants [62, 63]. Association of the receptor with its ligand results in conformational changes [64–66] so that as soon as binding sites of the receptor are occupied, this information is transferred to cytoplasm. Receptor binding to attractant and repellent molecules, and hence, the resulting changes in the frequency of switching between smooth swimming and tumbling are modulated by the rate of change of the number of bound receptors [67]. This rate can be represented as dp/dt where p is the value (averaged over all the receptors) of the function $p(t)$ which assumes the value of 1 when the receptor is bound and 0 when it is not. It is assumed [68] that

$$p = c(c + c_{1/2})^{-1}, \tag{1}$$

where $c_{1/2}$ is the concentration of bound molecules for which $p = 0.5$. A change in the number of bound receptors results in altered behaviour of bacteria [67]. That is why, a change in the tumbling frequency is proportional to dp/dt. As a result of this change, randomly walking bacteria gradually migrate in the direction of increasing attractant concentration.

The relationship between bacterial behaviour and the temporal derivative dp/dt implies that the bacterial cell must be able to compare current and recent values of p. In

other words, the cell's chemotactic response, i.e the signal modulating the tumbling frequency and denoted below as R, is proportional to the difference $(p-A)$:

$$R = g(p-A)\,, \tag{2}$$

where g is the proportionality constant and A is the level of adaptation. In turn [69, 70] A varies as follows:

$$\frac{dA}{dt} = \frac{p-A}{\tau}\,, \tag{3}$$

where τ is the adaptation constant. There is a correlation between the levels of adaptation A and methylation, i.e. binding of CH_3 group of integral-membrane methyl-accepting chemotaxis protein, MCP [71]. Adaptation of bacterial cells is related to enhanced methylation which is in turn triggered by association of cell receptors with attractant molecules [71, 72]. According to equation (3), $dA/dt = 0$ at $A = p$, that is the cell is fully adapted. Solution of equation (3) for $t \gg \tau$ has the form:

$$A(t) = \frac{\exp(-t/\tau)}{\tau}\int_0^t p(t')\exp\frac{t'}{\tau}\,dt'\,. \tag{4}$$

It follows from equations (2) and (4) that

$$R(t) = g\left[p(t) - \frac{1}{\tau}\int_0^t p(t')\exp\frac{t'-t}{\tau}\,dt\right]\,. \tag{5}$$

The first term in square brackets in expression (5), $p(t)$, is the number of bound receptors at a given moment. The second term is the function $p(t)$ averaged over the entire past, with a weighting factor exponentially decreasing with time. So, in fact, this factor describes bacterial memory. According to equation (5), information about the number of bound receptors is retained within time $(t-t')$ which does not significantly exceed the adaptation constant τ.

Finally, a further important property of living systems, including bacteria, is reproduction. Interestingly, solution of the reproduction problem was one of the first applications of mathematics to the description of biological processes. It dates back to 1202, when Leonardo of Pisa (Fibonacci) suggested a technique to calculate the annual increase in the population of rabbits reared from a single pair (a male and a female). A series in which each term equals the sum of the two foregoing ones is generally referred to as the Fibonacci series. Curiously enough: (1) the ratio of any term in the series to the foregoing one tends to the famous number 1.618 (the so-called golden section) and (2) an increase in the number of rabbits N can be described in terms of the exponential law:

$$N = 1.171\exp[0.4812(n-1)]\,,$$

where n is the number of the division cycle. Later, it became evident that numerical coefficients of such an exponent differ for different organisms and depend on the parameters of the environment.

Let us now try and answer the question: what will solve a relatively simple mathematical problem more quickly, a bacterial population or a TV automaton? Let us consider a surface of a definite size, e.g. 1 cm^2, on which a grid of M points is plotted (assuming a mesh size of 5 μm to be approximately equivalent to the length of a bacterial cell). N points out of this total number M are filled with an attractant. N is the unknown number to be found. 2×10^{13} bacterial cells are needed to cover all N points. Assuming the duration of the cell cycle to be 20 min, it is easy to determine the time necessary for this amount of bacterial cells to be produced; it is about 3 h. Bacteria travelling at a rate of 2 mm min^{-1} will spend altogether around 200 min to find N points. The search and the reproduction occur in parallel; therefore there is no appreciable increase in the total time needed to reveal all N points containing the attractant.

A TV automaton that analyses the surface line by line with the same apparent resolution of 5 μm will operate by searching for all $M = 2\times10^{15}$ points. If the time nedeed to search for one point is 10^{-9} s (a high performance automaton!), the total duration of the analysis will amount to 600 h.

Thus, 'poorly performing' bacteria require hundreds of times less time to solve the same problem. Time savings will increase with increasing area to be analysed according to the formula

$$\beta \cong \frac{\tau}{\theta}\frac{M}{\ln N}\,,$$

where τ is the time needed for the TV automaton to search for each of the M points, θ is the duration of a bacterial generation cycle, and N is the subset of informative points in set M. This formula demonstrates that the advantage of technical devices attributable to their enhanced performance (taken into account by the first factor) is more than counterbalanced by the reproduction and motility of bioorganisms (taken into account by the second factor). In the above example, the first and the second factors are assumed to be 10^{-12} and 10^{14}, respectively. Therefore, by using principles derived from the repertoire of bacterial behaviour we can significantly reduce the time of analysis.

1.3 Memory

Computers are known to keep information at least at three different levels: long-term memory (magnetic and optical tape, disk, and diskette storage), on-line storage (ferrite cores, triggers, etc), and dynamic memory (memory of the computing process, e.g. the presence or the absence of impulses in different parts of the chips). If the maximum lifetime of information is taken as 50 years (approximate life of magnetic tape) and its lower limit as 10^{-7} s (pulse duration), the temporal macrocycle of information storage in a technical device stretches over some 16 orders of magnitude.

Conformational changes of protein molecules (e.g. bacterial receptors) in living systems that serve as signals for external stimulus perception may also be regarded as a sort of dynamic memory. In this case, information is held for a span of picoseconds. On the other hand, hereditary memory stored in DNA molecules in the form of genetic code needs a few generations to undergo appreciable changes. Finally, live systems use intermediate memory mechanisms which enable them to keep information accumulated by individual organisms in the course of learning and stored in their neurons.

Bacteria have a relatively short memory which facilitates their adaptation to the environment [see equation (5)]. Adaptation depends on methylation of integral-membrane MCP. Bacterial memory may be regarded as a specific case of information storage. The concept of information storage was introduced to designate the period during which the system forgets noises that affected it [73]. Memory enables bacteria to compare, using receptors, attractant or receptor

levels at points located along the path of bacterial motion (chemotaxis effect). The information obtained by means of such comparison is used to control the frequency of tumbling responsible for migration of bacteria in the direction of optimal environmental conditions. This can give rise to a cooperative effect, namely formation of bacterial population autowaves. It is bacterial chemotaxis that is the basis of this cooperative effect.

A memory analog in physics are temporal correlations which may result, for instance, from the collisions of elastic non-correlated particles (note, however, that such collisions are equally effective in destroying the correlations).

Another memory analog is the refractory period in active physical, chemical, and biological media, i.e. in media with energy sources distributed in them. Human brain may be regarded as an example of such a medium [74, 75].

1.4 Autowaves

Active media can generate self-sustained waves (so-called autowaves) that maintain their characteristics (period, length, amplitude, and shape) provided conditions of the medium remain unaltered. These characteristics depend only on the local properties of active media and do not depend on the initial conditions. Examples of autowaves include combustion waves, nerve impulses, waves in a system of distributed tunnel junctions, etc. (see for instance Refs [76, 77]). The phenomenon of autowaves underlies most processes involved in information control and transmission in biological systems. A brief discussion of autowave properties is presented below.

The simplest type of active media is a one-component medium. The energy spent to maintain autowaves in such a medium is not replenished, and an autowave is in fact a wave of switching from the high-energy state to the low-energy one. The basic model used to describe one-component media is a variant of the Kolmogorov–Petrovskii–Piskunov parabolic equation [78]:

$$\frac{\partial u}{\partial t} = D\Delta u + f(u) \,,$$
$$u(-\infty) = u_3 \,, \quad u(+\infty) = u_1 \,, \tag{6}$$

where u is a variable describing the state of the medium, D is the diffusion coefficient, and f is a nonlinear function.

The basic model (6) is in a sense an antipode of classical wave systems including nonlinear ones. The latter systems in some way or other arise from the linear hyperbolic system

$$\frac{\partial^2 u}{\partial t^2} - \Delta u = 0 \,, \tag{7}$$

for which sinusoidal waves represent fundamental solutions. In contrast to equation (7), in the basic model (6) all wave processes are due to the dynamics of the nonlinear point system

$$\frac{\partial u}{\partial t} = f(u) \,, \tag{8}$$

which is actually or potentially an autooscillating system. Autowaves are in some respects radically different from waves described by hyperbolic equations. This is illustrated by Table 1.

Table 1. Comparison of wave and autowave properties [79]

Property	Waves	Autowaves
Conservation of energy	+	−
Conservation of amplitude and shape	−	+
Interference	+	−
Annihilation	−	+
Reflection	+	−
Diffraction	+	+

Symbols '+'and '−' indicate the presence and the absence of a given feature, respectively.

With the N-shaped dependence $f(u)$ inherent in many active media, there are two stable states associated with the left and right zeros of function $f(u)$, respectively (Fig. 4a). Under these conditions, the autowave can be regarded as a travelling wave front (Fig. 4b).

A substantially broader class of autowave processes is feasible in re-excitable active media where the travelling wave has finite duration; as soon as its propagation is over, the medium reverses to the initial state. Examples of such media are chains of coupled Van der Pol-type generators, nerve fibres, distributed chemical systems with an autocatalyst, etc. [76, 77, 79, 80]. The basic model of reexcitable active media can be represented by a system of two equations [81, 82]:

$$\tau_\theta \frac{\partial \theta}{\partial t} = l^2 \Delta\theta - q(\theta, \eta, A) \,, \tag{9}$$

$$\tau_\eta \frac{\partial \eta}{\partial t} = L^2 \Delta\eta - Q(\theta, \eta, A) \,, \tag{10}$$

where τ_θ, τ_η, l, and L are characteristic time periods and lengths, and A is a parameter characterising the level of system excitation. It is generally assumed that

$$\frac{\partial q}{\partial \theta} < 0 \,, \quad \frac{\partial Q}{\partial \eta} > 0 \,. \tag{11}$$

If conditions (11) for equations (9), (10) are fulfilled, then at $\theta = \text{const}$ fluctuations of the inhibitor are damped while at $\eta = \text{const}$ those of the activator grow. When studying various models of physical, chemical, and biological systems described by equations (9) and (10), simple functions are often taken for q and Q. For example [83–86],

$$q = \theta - B - A\theta^2\eta^{-1} \,, \quad Q = \eta - C\theta^2 \,, \tag{12}$$

or [87]

$$q = \theta - (B + \theta^2\eta)(I + A)^{-1} \,, \quad Q = \eta\theta^2 - A\theta \,, \tag{13}$$

or [77]

$$q = \theta^3 - \theta - \eta \,, \quad Q = \theta + \eta + \frac{2}{3^{3/2}} - A \,. \tag{14}$$

Models (12) and (14) have been originally intended to describe processes of morphogenesis, and model (13) is the well-known 'Brusselator'. For models (12)–(14), conditions (11) are fulfilled.

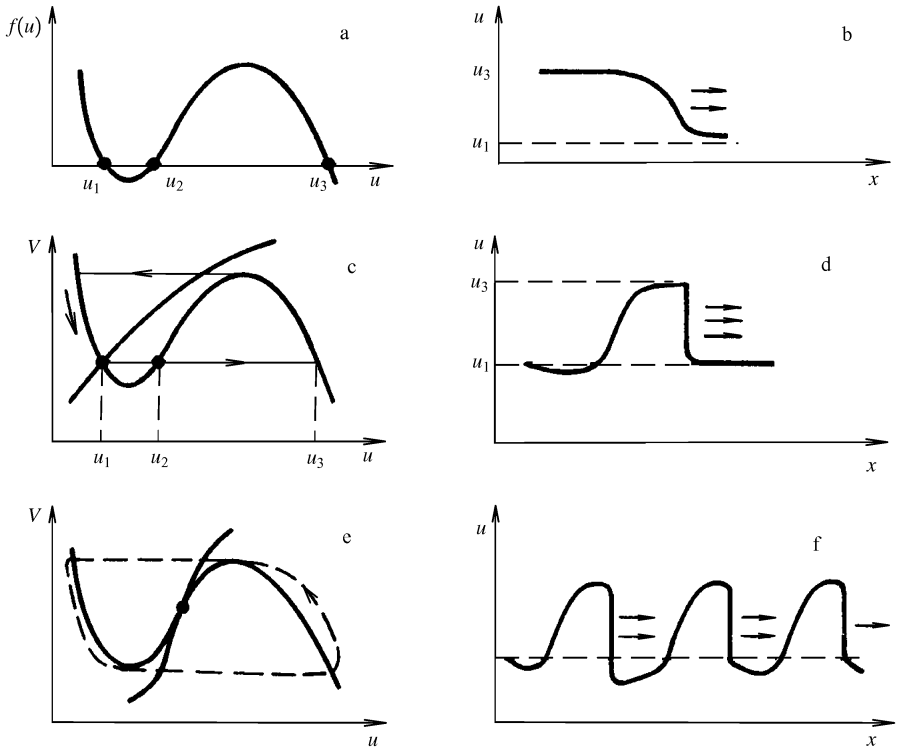

Figure 4. Travelling waves in models of excitable media: a, b — one-component model (1); c–f — two-component model (4), (5), where c, d is the waiting regime, and e, f is the autooscillation regime; $u \equiv \theta$, and $V \equiv \eta$.

The point system of equations

$$\tau_\theta \frac{\partial \theta}{\partial t} = -q(\theta, \eta, A) ,$$
$$\tau_\eta \frac{\partial \eta}{\partial t} = -Q(\theta, \eta, A) , \tag{15}$$

corresponding to equations (9)–(10) is normally a relaxation system with an N-shaped characteristic which may be either a waiting generator of unit pulses (Fig. 4c, d) or an autogenerator (Fig. 4e, f).

For chemical systems, $l \neq 0$ and $L \neq 0$; whereas for excitable cell membranes, $L = 0$. Variables in equations (9), (10) have the following meanings: for excitable membranes, θ is the potential on the membrane and η is the conductivity of the slow component of the ion flow; for a chemical excitable medium, θ and η are reagent concentrations.

Travelling waves are the simplest type of solutions for equations (9), (10). Such waves have their own characteristic velocity and amplitude, both dependent on the parameters of the medium and independent of the initial and boundary conditions. This is easy to demonstrate on the example of a one-dimensional variant of equation (6):

$$\frac{\partial u}{\partial t} = D\frac{\partial^2 u}{\partial x^2} + f(u) . \tag{16}$$

Upon substitution of variables $\xi = at - x$ (where a is the wave velocity), equation (16) assumes the form:

$$a\frac{du}{d\xi} = D\frac{d^2 u}{d\xi^2} + f(u) , \tag{17}$$

$$u(-\infty) = u_1 , \quad u(+\infty) = u_3 . \tag{18}$$

Standard substitution $du/d\xi = p$ converts equation (17) to the first order equation

$$Dp\frac{dp}{du} - ap + f(u) = 0 . \tag{19}$$

If $f(u)$ has the form of a cubic polynomial, i.e.

$$f(u) = -k(u - u_1)(u - u_2)(u - u_3) ,$$

then direct integration of equation (19) gives the wave velocity a [88]:

$$a = \sqrt{\frac{kD}{2}}(u_1 + u_3 - 2u_2) .$$

Solution in the form of a solitary autowave that propagates with velocity a corresponds to the separatrix proceeding from saddle u_1 to saddle u_3 (Fig. 5), i.e.

$$p = \text{const} \times (u - u_1)(u - u_3) .$$

The amplitude of such a wave is equal to the difference $u_3 - u_1$.

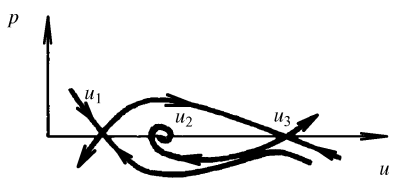

Figure 5. Trajectory in the phase plane of the one-component model.

The velocity of periodic waves depends on period T and falls with decreasing T [76, 77]. Results of analysis suggest stationary wave spreading is feasible only at $T > T_{min}$. Dependences of T_{min} and velocity of propagation of periodic autowaves on the parameters of the medium have been examined in Refs [89, 90]. At $T < T_{min}$, wave travelling patterns are very unusual in that the waves propagate without damping, but not all of them, because each third or fourth wave (depending on T) is missed out (fails to propagate) In two-dimensional nonhomogeneous media, this can be accompanied by disruption of the wave front. Further evolution of such disruptions frequently results in the formation of additional wave sources (reverberators) [76, 77, 79].

The existence of T_{min} is due to the fact that autowaves cannot spread until rehabilitation processes described in equations (9), (10) by the slow temporal variable η are completed. The characteristic time of recovery is referred to as refractoriness and is related to the motion of a point along the left branch of isocline $\dot{\theta} = 0$ (Fig. 4c).

Therefore, the medium appears to 'remember' a recent event, i.e. propagation of the autowave front, during the refractory period until its excitability is fully restored. It is this circumstance that allows refractoriness to be considered as a physical analog of memory.

Refractoriness appears to be responsible for annihilation of colliding autowaves (Table 1). In an excitable medium, the autowave front (represented on the phase plane by the shift from the left descending branch of isocline $\dot{\theta} = 0$ to the right one; see Fig. 4c, e) is followed by a refractory trailing edge, i.e. an unexcitable zone (zone of slow motion in the phase plane). This accounts for reciprocal impermeability of two autowaves, their annihilation, and the absence of reflection from the boundaries of the excitable medium.

Specific features of autowave phenomena simulated by equations (9) and (10) are largely due to refractoriness ('memory' of the active medium). However, these equations do not describe the whole gamut of autowave types and properties. Specifically, they do not characterise autowaves generated by elements that have their own memory, e.g. population autowaves.

A fundamental mathematical feature of autowaves generated by elements with memory is that they can be characterised by function q dependent not only on functions $\theta(x, y, t)$ and $\eta(x, y, t)$ as in equations (9), (10) but also on spatial derivatives of these functions [13, 91]. Therefore, on the basis of formal characteristics alone such autowaves may be categorised as representing a separate class [91].

Does this class have anything in common with other types of autowaves? What new specific effects can arise from individual elements possessing memory? In this review we present recent findings pertinent to such effects and demonstrate their important role in the formation, propagation, and functioning of population autowaves as well as in the development of diffusional instability and morphogenesis (formation of spatial structures).

2. Population autowaves as a cooperative response of chemotactic bacterial cells

2.1 Phenomenological model

In the mid-1960s, Adler and co-workers demonstrated that local inoculation of bacteria into the nutrient medium gives rise to propagating population waves (Fig. 6) [31, 92–95]. It was further shown that these waves may be regarded as a macroscopic phenomenon that results from microeffects of bacterial memory — specifically, from tumbling rate alteration in individual cells induced by a change in the attractant level. A local decrease in attractant concentration is due to its consumption by bacteria which eventually produces a concentration gradient. It is possible to single out in the chaotic motion of bacteria a governing constituent oriented along the gradient. This, combined with continuing reproduction of bacteria, generates autowaves easily discernible with the naked eye. In fact, autowaves make visible the boundary between the zone with decreased attractant concentration (e.g. inside a broadening circular bacterial front in Fig. 6) and another zone where attractant concentration remains elevated [25, 31, 92–95].

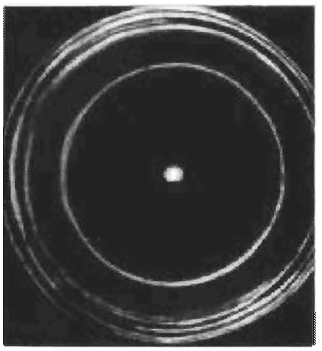

Figure 6. Bacterial population wave in a Petri dish [25].

A mathematical model describing autowave propagation was first suggested in 1971 [96, 97].

Let $f(c)$ be the mean tumbling frequency in cells proceeding in a given direction, c — the mean concentration of attractant consumed by bacteria which is a function of coordinate x (in one-dimensional case), and $b(x)$ — bacterial cell density in point x. Then, the cell flow $J(x)$ in the direction of growing x, per unit of time, may be represented by the expression [96]:

$$J(x) = \int_{x-\Delta}^{x} f\left[c\left(s+\frac{1}{2}\alpha\Delta\right)\right] b(s)\,\mathrm{d}s - \int_{x}^{x+\Delta} f\left[c\left(s-\frac{1}{2}\alpha\Delta\right)\right] b(s)\,\mathrm{d}s\,, \qquad (20)$$

where α is the ratio of the effective length of the cell to the distance Δ which the cell covers in a unit of time unit. The effective length of a bacterial cell is thus $\alpha\Delta$. Using an approximation which is frequently employed in basic studies of Brownian motion [98], we can write equation (20) as:

$$J(x) \cong \Delta^2 \left\{ -f[c(x)] \frac{\mathrm{d}b}{\mathrm{d}x} + (\alpha - 1) \frac{\mathrm{d}f}{\mathrm{d}c} b(x) \frac{\mathrm{d}c}{\mathrm{d}x} \right\},$$

or (in this approximation)

$$J(x) = -\mu \frac{\mathrm{d}b}{\mathrm{d}x} + \chi b \frac{\mathrm{d}c}{\mathrm{d}x}\,. \qquad (21)$$

In formula (21), motility of bacterial cells is defined by the coefficient

$$\mu(c) = \Delta^2(\Delta t)^{-1} = f(c)\Delta^2 , \tag{22}$$

where $\Delta t = 1/f(c)$ is the mean time interval between two successive tumbling episodes. Chemotactic bacterial response to a change in the environment is characterised by the coefficient

$$\chi(c) = (\alpha - 1)\Delta^2 \frac{\mathrm{d}f}{\mathrm{d}c} , \tag{23}$$

where $\mathrm{d}f/\mathrm{d}c$ describes altered behaviour of bacteria attributable to their short-term memory. It follows from equations (22) and (23) that

$$\chi(c) = (\alpha - 1)\frac{\mathrm{d}\mu}{\mathrm{d}c} .$$

Since

$$\frac{\partial b}{\partial t} = -\vec{\nabla}\boldsymbol{J} ,$$

where [99]

$$\boldsymbol{J} = -\mu\vec{\nabla}b + \chi b\vec{\nabla}c ,$$

we have (for the one-dimensional case)

$$\frac{\partial b}{\partial t} = -\frac{\partial}{\partial x}\left(-\mu\frac{\partial b}{\partial x} + \chi b\frac{\partial c}{\partial x}\right) . \tag{24}$$

The first term in the right-hand side of equation (24) represents non-chemotactic bacterial motion whereas the second term describes the chemotactic response of bacterial cells.

The nutrient substrate level, i.e. the concentration of the attractant, changes as described by the modified diffusion equation:

$$\frac{\partial c}{\partial t} = -k(c)b + D\frac{\partial^2 c}{\partial c^2} , \tag{25}$$

where the first term in the right-hand side characterises consumption of the substrate by bacterial cells and D is the substrate diffusion coefficient. It is generally assumed that substrate concentration is sufficiently high and is not a limiting factor of the consumption rate, that is $k(c) = k_0 = \text{const}$. If we further assume that $\mu(c) = \mu_0 = \text{const}$ and $\chi(c) = \delta/c$ in equation (24) (in accordance with the Weber–Fechner law maintaining that the response to a stimulus is proportional to its relative strength) and $D = 0$ in equation (25) we get [97]

$$b(\xi) = \frac{u^2 c_\infty}{\mu_0 k_0(\bar{\delta} - 1)} \exp(-\bar{\xi})\left[1 + \exp(-\bar{\xi})\right]^{-\bar{\delta}/(\bar{\delta}-1)} , \tag{26}$$

$$c(\xi) = c_\infty\left[1 + \exp(-\bar{\xi})\right]^{-1/(\bar{\delta}-1)} , \tag{27}$$

where $\bar{\xi} = (u/\mu_0)\xi$ (u being the constant population wave velocity), $\xi = x - ut$, and $\bar{\delta} = \delta/\mu_0$. Solution (26)–(27) has been obtained with the following boundary conditions:

$$b \to 0 , \quad \frac{\mathrm{d}b}{\mathrm{d}\xi} \to 0 , \quad c \to c_\infty \quad \text{when} \quad |\xi| \to \infty .$$

Such a solution is sufficiently accurate to describe uniform (along a capillary) propagation of local cell compaction (population wave) observed experimentally [93] which is due to (a) attractant consumption by bacteria and (b) bacterial chemotactic response (functionally related to short-term memory) to the continuously generated attractant concentration gradient in the wave front zone.

In equation (24), the chemotactic response is defined by the expression $V_{\mathrm{ch}}b$ where

$$V_{\mathrm{ch}} = \chi\frac{\partial c}{\partial x} \tag{28}$$

is the so-called chemotactic velocity.

Subsequently, that is since 1971, the expression for V_{ch} has undergone substantial changes in line with new experimental data. For example, in the exponential attractant gradient, formula (28) with the assumption

$$X(c) = \frac{\delta}{c}$$

predicts $V_{\mathrm{ch}} = \text{const}$, whereas it has been experimentally found that the chemotactic velocity undergoes marked changes under these conditions [100]. Having analysed experimental findings, Scribner et al. modified function $\chi(c)$ in such a way that $\chi(c) \to 0$ when $c \to 0$ provided concentration c of the consumed attractant is below a certain threshold level [101]. In 1976, Lapidus and Schiller proposed a new form for function V_{ch} [102]:

$$V_{\mathrm{ch}} = \delta\left(\frac{\mathrm{d}}{\mathrm{d}c}\frac{c}{k + c}\right)\frac{\mathrm{d}c}{\mathrm{d}x} , \tag{29}$$

where $\delta = \text{const}$ and k is a constant determining chemotactic sensitivity, i.e. dissociation constant of the attractant–receptor complex. Expression (29) is in perfect agreement with experimental results demonstrating proportionality of chemotactic response to the gradient of function f of attractant concentration at $f = c/(k + c)$ [103]. Nevertheless, the form of function f turned out to be in need of further correction because chemotactic response at high attractant levels (more than 10 mM in the case of serine) does not become saturated but continues to increase [104]. In agreement with this feature of chemotactic response, it was suggested [105] that

$$V_{\mathrm{ch}} = \chi_M\left(\frac{\mathrm{d}}{\mathrm{d}c}\frac{c^n}{k^n + c^n}\right)\frac{\mathrm{d}c}{\mathrm{d}x} , \quad n = \frac{1}{2} . \tag{30}$$

The form of function (30) may reflect the presence of a heterogeneous population of receptors with different chemical affinity for the same attractant [105]. Finally, Boon and Herpigny [106] suggested a mathematical model allowing a description of the chemotactic responses of bacterial cells to more than one chemical stimulus. In this case

$$V_{\mathrm{ch}} = v_0\sum_i\left[\frac{\mathrm{d}}{\mathrm{d}c_i}\frac{(c_i/c_i^{\mathrm{s}})^2}{1 + (c_i/c_i^{\mathrm{s}})^2}\right]\frac{\mathrm{d}c_i}{\mathrm{d}x} , \tag{31}$$

where v_0 is the so-called 'chemotactic potential' and c_i^{s} is a certain threshold attractant level.

2.2 Zavalskii's theory

Evidently, model (24), (25) where $V_{\mathrm{ch}} = (\delta/c)\partial c/\partial x$ and its modifications (29)–(31) have phenomenological character. In the mid-1980s, Zavalskii and co-workers deduced equations (24), (25) from more fundamental kinetic equations [107–109].

In accordance with the Zavalskii model, the propagation of a bacterial population wave can be described by the following equation [108]:

$$\frac{\partial f(\boldsymbol{r}, \boldsymbol{n}, t)}{\partial t} + V\boldsymbol{n}\nabla f(\boldsymbol{r}, \boldsymbol{n}, t) = -\gamma\left(V, \boldsymbol{n}, \frac{\partial c}{\partial t}, \nabla c\right) f(\boldsymbol{r}, \boldsymbol{n}, t) + \frac{1}{4\pi}\int_{\boldsymbol{n}} \gamma\left(V, \boldsymbol{n}, \frac{\partial c}{\partial t}, \nabla c\right)\beta(\boldsymbol{n}, \boldsymbol{n}')f(\boldsymbol{r}, \boldsymbol{n}', t)\,\mathrm{d}\boldsymbol{n}' , \quad (32)$$

where f is the density of distribution of the cells migrating in direction $\boldsymbol{n}$ in the infinitely small vicinity of point $\boldsymbol{r}$ at time t, γ is the tumbling rate, and $\beta(\boldsymbol{n}, \boldsymbol{n}')$ is the probability that a bacterial cell that migrated by means of smooth swimming in direction $\boldsymbol{n}$ will be reoriented in direction $\boldsymbol{n}'$ after tumbling. In compliance with the Zavalskii model [109], it is assumed that chemotactic velocity is determined by equation (29) and characterised by a change in the relative number, N, of receptors bound to attractant molecules. In other words:

$$\frac{\mathrm{d}N}{\mathrm{d}t} = \frac{k}{(k+c)^2}\frac{\mathrm{d}c}{\mathrm{d}t} , \quad (33)$$

where (for a one-dimensional case) [103]

$$\frac{\mathrm{d}c}{\mathrm{d}t} = \frac{\partial c}{\partial t} + Vv\frac{\partial c}{\partial x} . \quad (34)$$

In equation (34), $V = \text{const}$ is the speed of bacterial motion in a medium with a constant chemoeffector concentration gradient, v is the cosine of the angle between the gradient and axis x, while $\partial c/\partial t$ is defined by equation (25). It follows from equations (33) and (34) that

$$\frac{\mathrm{d}N^*}{\mathrm{d}t} = \frac{kN_0}{(k+c)^2}Vv\frac{\partial c}{\partial x} , \quad (35)$$

where N^* is the absolute number of bound receptors and N_0 is the total number of receptors in a given chemoeffector. Formula (35) was derived with the condition that $\partial c/\partial t \ll Vv\,\partial c/\partial x$ [109], in agreement with the available experimental data. Going over from equation (33) to equation (35) is in fact equivalent to the change from 'temporal' to spatial reception.

In accordance with experimental findings [68], function γ from equation (32) can be defined as follows:

$$\gamma = \gamma_0 \exp\left(-\alpha\frac{\mathrm{d}N^*}{\mathrm{d}t}\right) , \quad (36)$$

where α is the proportionality coefficient dependent on both the bacterial strain and the type of receptor (i.e. nutrient substrate consumed by bacteria). With equation (35) in mind, we can write formula (36) as

$$\gamma = \gamma_0 \exp(-\Psi v) , \quad (37)$$

where

$$\Psi = \frac{\alpha N_0 k}{(k+c)^2}V\frac{\partial c}{\partial x} . \quad (38)$$

'Microscopic' parameters included in formula (38) can, in principle, be determined experimentally.

To obtain function $\beta(\boldsymbol{n}, \boldsymbol{n}')$ from equation (32), Zavalskii [109] used results of experimental studies reported by Berg and Brown [23]. He approximated function β by the following cubic polynomial:

$$\beta(\boldsymbol{n}, \boldsymbol{n}') = 3\pi(1 + 4\langle \boldsymbol{n}, \boldsymbol{n}'\rangle - \langle \boldsymbol{n}, \boldsymbol{n}'\rangle^2 - 4\langle \boldsymbol{n}, \boldsymbol{n}'\rangle^3) , \quad (39)$$

where $\langle \boldsymbol{n}, \boldsymbol{n}'\rangle$ is the cosine of the angle between vectors $\boldsymbol{n}$ and $\boldsymbol{n}'$.

Upon substitution of formulas (37) and (39) into equation (32), it is possible to obtain, in diffusional approximation [109]:

$$\frac{\partial b}{\partial t} - \frac{V}{3}\frac{\partial}{\partial x}\left[\frac{1}{\omega_1^1}\left(V\frac{\partial b}{\partial x} + \omega_0^1 b\right)\right] = 0 , \quad (40)$$

where

$$\omega_0^1 = -\frac{1}{5}\left(\Psi + \frac{1}{10}\Psi^3 + \frac{1}{280}\Psi^5 + \frac{1}{15120}\Psi^7 + \ldots\right) , \quad (41)$$

$$\omega_1^1 = \frac{1}{5}\left(1 + \frac{1}{6}\Psi^2 + \frac{1}{120}\Psi^4 + \frac{1}{5040}\Psi^6 + \ldots\right) + \frac{2}{75}\left(\Psi^2 + \frac{1}{14}\Psi^4 + \frac{1}{504}\Psi^6 + \ldots\right) , \quad (42)$$

and b is the bacterial cell concentration. Interestingly, equation (40) with coefficients (41) and (42) was derived without any constraints as regards the magnitude of the substrate (chemoeffector) concentration gradient which, in accordance with formula (38), determines function Ψ in equalities (41) and (42). Specifically, if the derivative $\partial c/\partial x$ is so small that $\Psi \ll 1$, the high-order terms in expansions (41) and (42) may be neglected; in this case equation (40) can be simplified to the expression [109]:

$$\frac{\partial b}{\partial t} - \frac{5V^2}{3\gamma_0}\frac{\partial^2 b}{\partial x^2} + \frac{V}{3}\Psi\frac{\partial b}{\partial x} + \frac{V}{3}\frac{\partial \Psi}{\partial x}b = 0 . \quad (43)$$

The form of equation (43) coincides with that of the phenomenological equation (24), but the two equations differ in that all functional parameters of equation (43) have a clearly defined physical meaning. At $\Psi \geqslant 1$, the change from equation (40) to equation (43) may not be legitimate. This being the case, coefficients μ and χ used in equation (24) cannot be expressed through simple analytical functions of parameters of an individual bacterial cell.

2.3 Rivero's theory

Another attempt to describe migration of bacterial populations in terms of individual cell properties was undertaken by Rivero et al. [110]. These authors managed to obtain formulas that relate bacterial motility coefficient μ [see equation (22)] and chemotactic velocity to the speed of individual bacteria and probability of their tumbling. A brief discussion of this approach follows below.

In a one-dimensional model, where V is the speed of bacteria while n^+ and n^- are the numbers of cells travelling in directions $+x$ and $-x$ respectively, V is $1/\sqrt{3}$ of the true speed of bacterial cells [111]; p^+ is the probability that a cell swimming in direction $+x$ will undergo tumbling and be reoriented. For a cell migrating in the opposite direction $-x$, the corresponding probability is p^-. It follows from the fact that the total cell number b remains unaltered (in the absence of reproduction) that:

$$\frac{\partial n^+}{\partial t} + \frac{\partial}{\partial x}(Vn^+) = p^-n^- - p^+n^+ , \quad (44)$$

$$\frac{\partial n^-}{\partial t} - \frac{\partial}{\partial x}(Vn^-) = p^+n^+ - p^-n^- , \quad (45)$$

$$b = n^+ + n^- , \quad (46)$$

$$J = V(n^+ - n^-) , \quad (47)$$

where J is the bacterial cell flow [a different definition has been given earlier, see formula (20)]. From equations (44)–(47), it is easy to obtain the expression:

$$\frac{\partial J}{\partial t}-\frac{1}{V}J\frac{\partial s}{\partial t}=-J(p^{+}+p^{-})-V\frac{\partial}{\partial x}(Vb)-Vb(p^{+}-p^{-})\,. \tag{48}$$

Suppose that the speed V does not depend on the attractant level which is true for a broad concentration range [22, 112]. Also suppose that the bacterial cell flow attained equilibrium [the time required for this must significantly exceed $(p^{+}+p^{-})^{-1}$]. In this case, it follows from equation (48) that

$$J=-\frac{V^{2}}{p^{+}+p^{-}}\frac{\partial b}{\partial x}+\frac{V(p^{-}-p^{+})}{p^{+}+p^{-}}b\,. \tag{49}$$

The form of formula (49) is similar to the phenomenological expression

$$J=-\mu\frac{\partial b}{\partial x}+V_{\mathrm{ch}}b\,, \tag{50}$$

which is easy to obtain from equation (24) and equality (28). Direct comparison of formulas (49) and (50) indicates that

$$\mu=\frac{V^{2}}{p^{+}+p^{-}}\,, \tag{51}$$

$$V_{\mathrm{ch}}=\frac{V(p^{-}-p^{+})}{p^{+}+p^{-}}\,. \tag{52}$$

Formulas (51) and (52) demonstrate the functional relationship between the 'macroscopic' quantities μ and V_{ch} on the one hand and individual cell parameters V, p^{+}, and p^{-} on the other. Also, μ and V_{ch} can be expressed through a change in the relative number N of bacterial cell receptors bound to attractant molecules. This will require the following assumptions:

(a) In a general case, a change in the number N of bound receptors may be caused by changing attractant concentration with time and by its spatial change in the vicinity of the bacterial cell swimming with speed V. Therefore:

$$\frac{\mathrm{d}N}{\mathrm{d}t}=\frac{\partial N}{\partial t}+V\frac{\partial N}{\partial x}\,. \tag{53}$$

(b) The direction of cell motion after a tumbling episode is over is not totally random [23] which accounts for [113]

$$p^{+}/p^{-}=\gamma\frac{1-\varphi}{2} \tag{54}$$

(for *Escherichia coli* exhibiting chemotactic response to a changing concentration of an aminoacid, the value of φ is close to 0.3 [113]). In formula (54) and equation (32) γ is the tumbling frequency.

(c) In accordance with formula (36)

$$\gamma=\gamma_{0}\left(-\alpha_{0}\frac{\mathrm{d}N}{\mathrm{d}t}\right)\,, \tag{55}$$

where $\alpha_{0}=\alpha N_{0}$ [N_{0} is the total number of receptors of a given chemoeffector; the same notation was used in formula (35)].

Substitution of equations (53) and (55) into formula (54) and then of the resulting expression into formulas (51) and (52) gives the following final equation [110]:

$$\mu=\frac{V^{2}}{(I-\varphi)\gamma_{0}}\exp\left(\alpha\frac{\mathrm{d}N}{\mathrm{d}c}\frac{\partial c}{\partial t}\right)\operatorname{sech}\left(\alpha V\frac{\mathrm{d}N}{\mathrm{d}c}\frac{\partial c}{\partial x}\right)\,, \tag{56}$$

$$V_{\mathrm{ch}}=V\tanh\left(\alpha V\frac{\mathrm{d}N}{\mathrm{d}c}\frac{\partial c}{\partial x}\right)\,. \tag{57}$$

The quantity $\mathrm{d}N/\mathrm{d}c$ in formulas (56) and (57) stands for changes in the number of bound receptors due to changing attractant concentration. According to equation (33)

$$\frac{\mathrm{d}N}{\mathrm{d}c}=\frac{k}{(k+c)^{2}}\,, \tag{58}$$

where k is the dissociation constant for the attractant–receptor complex.

Both Zavalskii's and Rivero's models make it possible to describe the effect of bacterial memory underlying chemotactic responses of individual cells on the formation of macroscopic dynamic structures, i.e. population waves. The object of future studies will be to clarify the relationship between these models and the results of *in vivo* experiments. Of special interest in this context are findings reported in Ref. [114] which indicate that Rivero's model compares very well with earlier experimental observations [100] in that it actually describes both the profile of bacterial population waves and the relationship between wave propagation velocity and concentration of the attractant substrate.

To summarise, let us note that equations (40) and (43) obtained by Zavalskii as well as Rivero's equation (49) may, strictly speaking, be applied only to the analysis of one-dimensional regimes of population wave propagation. Nevertheless, the epistemological importance of these theories can scarcely be exaggerated since they provide the theoretical basis for phenomenological equations such as (24), (25), and the like. Extrapolation of the results obtained by the analysis of one-dimensional models to two- and three-dimensional cases (accomplished artificially, e.g. by a $\sqrt{n}$-fold reduction of the cell speed, where n is dimensionality [115]) has no solid theoretical basis. At the same time, it is in reasonable agreement with the available experimental findings [116, 117].

All in all, there remains much work to be done to complete theory of autowaves generated by structures with memory elements.

3. Interaction between bacterial population waves and formation of static spatial structures

3.1 Ω and KΩ structures

It has been demonstrated in the foregoing discussion that motile bacterial cells inoculated into semisolid agar medium can generate wave fronts with enhanced cell density. Migration of such fronts can be regarded as autowave propagation and described by autowave 'reaction–diffusion' equations [91, 107–110, 118].

Interestingly, bacterial waves closely approaching each other have been found to induce the formation of motionless stationary structures referred to as demarcation zones. Such zones separate different bacterial populations and prevent the formation of a solid bacterial lawn [119–121].

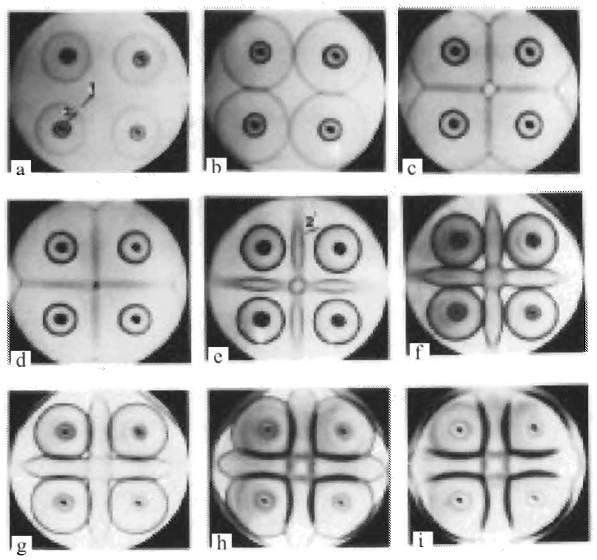

Figure 7. Formation of bacterial Ω-like structures [123]: a — approaching chemotaxis rings; b–d — their collision; e — their reflection from the collision zone; f — collision of reflected autowaves with the second tide of chemotaxis waves; g–h — formation of a stationary cross-like structure.

It has been reported [121] that demarcation zones may result from the collision of bacterial fronts (chemotaxis rings) and their subsequent reciprocal reflections. In such cases, demarcation zones are located along front collision lines (Fig. 7). Both reflection and emission of several successive bacterial autowave fronts are the results of the ability of bacteria to switch over from selective consumption of one substrate (the concentration of which in the inoculation zone and in the zone where the fronts draw together falls almost to zero) to the consumption of another [13, 122]. The resulting stationary demarcation zones will be further referred to as Ω structures [123].

Another type of demarcation zones, the so-called KΩ-like structures [124], has been reported to occur in experiments where wave fronts (chemotaxis rings) formed by separate bacterial communities cannot come into direct contact [119, 120] and consequently do not collide (Fig. 8).

Therefore, bacterial communities converging as a result population autowave propagation can give rise to two types of static spatial structures, Ω and KΩ. It is noteworthy, that transition from Ω structures to KΩ structures can be induced by impaired bacterial cell motility (e.g. owing to an increase in agar density).

Unlike Ω structures, KΩ structures are formed as a result of breaches in the approaching fronts; these fronts then diverge in directions perpendicular to the line that connects these wave sources (inoculation points) and thus 'trace' the boundaries of the demarcation zone (Fig. 8a–c). The second tide of chemotaxis rings following the first one is similarly unable to spread beyond the demarcation zone (Fig. 8d). The zone remains apparent even 10–15 hours after its formation (Fig. 8f).

The above mechanisms for demarcation zone formation are responsible for different spatial structures generated by population waves approaching each other. Formation of Ω-like structures is associated with enhanced bacterial density at points where chemotaxis rings intersect, as compared with cell density in those zones of the nutrient medium where they do not (Fig. 7b). Formation of KΩ structures does not produce a similar effect.

We have demonstrated that the type of structure is determined by various external factors including both agar concentration and initial pH values of the nutrient medium. Fig. 9 presents the results of experiments showing the formation of different structures (Ω or KΩ) in relation to pH and agar density in the nutrient medium. One can

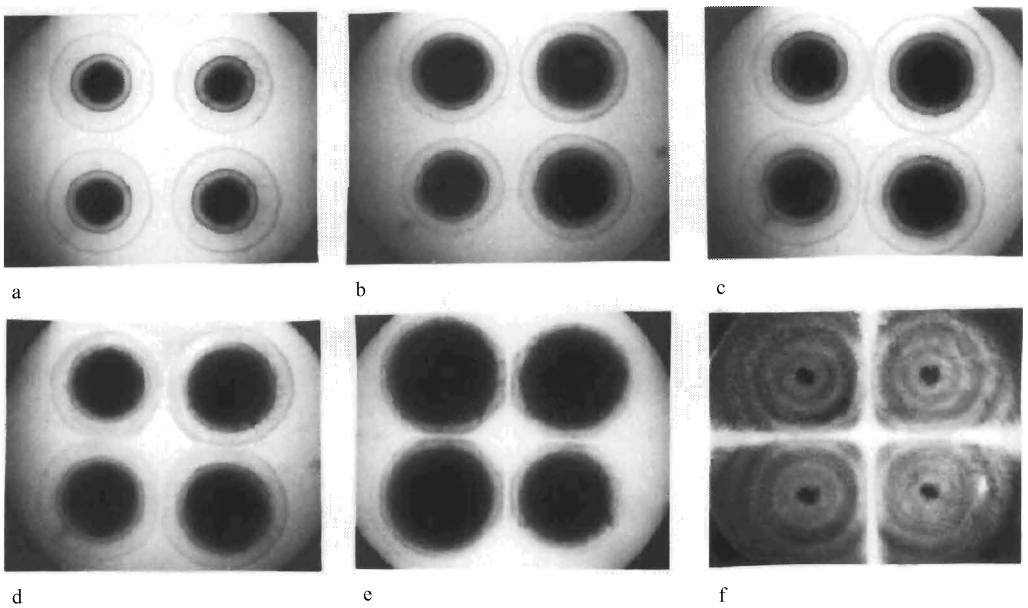

Figure 8. Formation of bacterial KΩ-like structures: a — two chemotaxis rings spreading from inoculation points [125]; b, c — formation of cross-like wave patterns as bacterial population waves converge; d — chemotaxis rings of the second tide unable to penetrate the demarcation zone; e — bacterial growth area spreading behind chemotaxis rings and equally incapable of entering the demarcation zone. Note prominent stationary rings within each bacterial growth zone which suffer breaches at the boundaries of the demarcation zone.

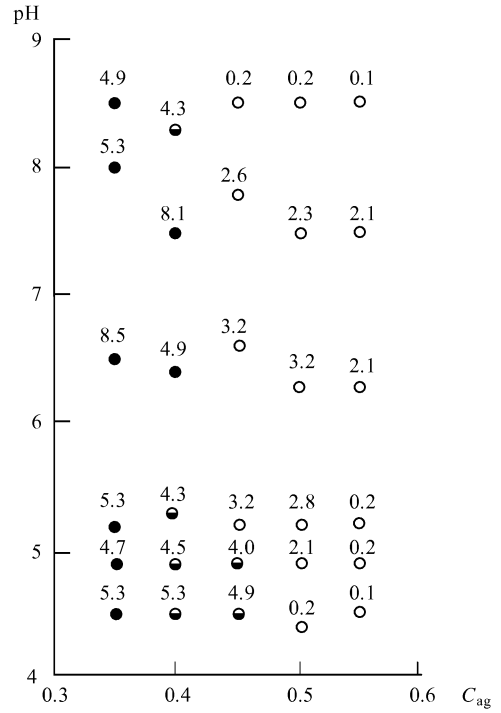

Figure 9. Relationship between parameters of the medium (pH and agar density C_{ag}) and the type of structures arising from autowave interaction of approaching chemotactic populations of *E. coli* [125]. Shaded and open circles denote Ω and KΩ structures, respectively. Half-shaded circles denote regimes at which the structure type depends not only on pH and C_{ag} but also on the distance between inoculation points. Figures above the circles indicate mean velocities of propagation of corresponding chemotaxis rings (mm h^{-1}).

clearly see two characteristic regions for each structure. Formation of KΩ-like structures is associated with a lower rate of expansion of chemotaxis rings than that of Ω-like structures. The fronts do not collide if their average velocity is lower than the critical value of about 4 mm h^{-1} [124]. Specifically, population fronts generated by *Halobacterium halobium* never collide because their velocity is at least one order of magnitude lower than the critical value [125]. Nor do they form Ω-like structures.

Transition from one type of structure to the other following a change in the parameters of the nutrient medium (e.g. C_{ag} and pH) may be due to the change of its global properties independent of bacterial activity (its structure, viscosity, etc.) as well as local changes induced by the microorganisms themselves. The latter cause has been reported [124] to be the determining one in that the modulating effect of bacteria on the nutrient medium where the wave fronts converge appears to be responsible for the formation of different spatial structures. The nature of this effect required a special study.

It was hypothesised that the type of structure may be related to bacterial motility which is in turn controlled by environmental conditions (C_{ag} and pH) [124]. Fig. 9 shows that formation of KΩ structures, unlike that of Ω structures, occurs at a low propagation velocity of chemotaxis rings, possibly owing to impaired motility of bacteria at certain pH and agar density values (Fig. 9). Concurrently, chemotaxis ring contrast at lower than critical propagation rates is markedly reduced and decreases with increasing ring diameter. This would suggest that the formation of KΩ structures is associated not only with reduced bacterial motility but also with a fall in the bacterial reproduction rate. Reduced bacterial motility facilitates the growth of the concentration of repellents, products of metabolism, just ahead of the slowly migrating chemotaxis ring. These compounds may be responsible for initiating negative taxis in bacteria and can prevent wave fronts from coming into close contact [124], either directly or through local changes in the pH of the nutrient medium. The latter mode of action appears to be very likely in view of pH changes in zones where bacterial population waves propagate [126, 127]. Another feasible mechanism by which KΩ structures could be generated is the lack of nutrient substrate just in front of slowly approaching chemotaxis rings [128]. Special studies revealed mechanisms of morphogenesis caused by approaching population autowaves, both Ω and KΩ ones.

Interestingly, the notion of KΩ and Ω autowaves was first introduced to describe autowaves generated by elements devoid of memory. Such autowaves (e.g. concentration waves in the Belousov–Zhabotinskii reaction [76, 77, 79, 81, 82, 129–131]) can be described by equations (4) and (5).

Kerner and Osipov [81] have demonstrated that equations (4) and (5) describe two essentially different types of autowaves with $\varepsilon = l/L$ as the governing parameter. The properties of such autowaves propagating in a medium with $\varepsilon \ll I$ (KΩ autowaves) are radically different from those of autowaves travelling in a medium where $\varepsilon > 1$, or Ω-like autowaves [81]. It is known that converging Ω-like waves annihilate [76, 77, 79, 87, 129–134] whereas KΩ-like waves do not [81]. This difference can be accounted for by the fact that in the case of KΩ waves $L \gg l$, which means that 'a diffusion forerunner' (a refractory region $\sim L$ in size) propagates in front of the KΩ wave [81, 135]. As a result, two con-verging KΩ waves begin to interact at distances considerably exceeding the front width ($\sim l$).

The question arises: can a mathematical model of bacterial population waves (i.e. autowaves generated by cells possessing memory and, hence, chemotaxis) describe both Ω and KΩ waves? The answer is not obvious. Indeed, such a model is substantially different from the simple mathematical model represented by equations (9) and (10). To demonstrate this, we shall consider the following model of bacterial population autowaves [118]

$$\frac{\partial b}{\partial t} = r(p)b + \nabla\left[\lambda(p)\nabla b - v\nabla\left(\chi(p)b\nabla p\right)\right], \tag{59}$$

$$\frac{\partial p}{\partial t} = -r(p)b + \Delta p, \tag{60}$$

where

$$\nabla \equiv \frac{\partial}{\partial x} + \frac{\partial}{\partial y}, \quad \Delta \equiv \frac{\partial^2}{\partial x^2} + \frac{\partial^2}{\partial y^2},$$

t is time, b is bacterial cell density, and p is concentration of the attractant consumed by bacteria. The first term in equations (59) and (60) describes growing cell number and substrate consumption by bacteria, respectively. The rate of cell number growth is

$$r(p) = \frac{p}{p + P_r}, \tag{61}$$

where P_r is Monod's constant [131]. The second term in

equation (59) describes chaotic bacterial motion in the absence of chemotactic effects. The motility of bacteria is

$$\lambda(p) = \begin{cases} \lambda_0 & \text{at } p > p_0, \\ \lambda_0 \dfrac{p}{p_0} & \text{at } p \leqslant p_0, \end{cases} \tag{62}$$

where p_0 and λ_0 are constants . It follows from formula (62) that a fall in substrate concentration p (at $p \leqslant p_0$) is accompanied by a decrease in bacterial motility. The third term in equation (59) describes chemotactic response of bacterial cells to the substrate-chemoeffector gradient ∇p. If the chemoeffector is an attractant, the cells compare its concentration at adjacent points of the nutrient medium [bacterial memory effect, see formula (5)] and gradually migrate to the region with higher concentration p. The constant v describes the intensity of bacterial chemotactic response, while $\chi(p)$ is the chemotactic sensitivity of the cells. It is characterised by the following functional dependence:

$$\chi(p) = \begin{cases} 1/p \text{ or } P_k/(p+P_k)^2 & \text{at } p > p_0, \\ \dfrac{(p/p_0)^i}{p} & \text{at } p \leqslant p_0, \end{cases} \tag{63}$$

where P_k is the dissociation constant of membrane receptors of a given bacterial chemoeffector.

It is obvious from equations (59)–(62) that migration of bacterial population autowaves depends not only on functions $b(x, y, t)$ and $p(x, y, t)$ but also on their spatial derivatives. This is an important but not the sole difference of model (59), (60) and similar models [e.g. (24), (25)] from the classical models (4)–(9). For example, chaotic bacterial motion is characterised by the functional dependence $\lambda(p)$ [see formula (62)] rather than by a constant, unlike chaotic motion of reagent molecules which is described by diffusion terms in equations (4), (5). Moreover, in contrast to model (9)–(14), where it is usually assumed that $\tau_\theta \ll \tau_\eta$ [81], in model (59), (60) the characteristic time of changes in bacterial density b is taken to be of the same order of magnitude as the characteristic time of changes in nutrient substrate concentration p.

Numerical solution of equations (59)–(63) indicates that this model of propagation of bacterial population waves can describe both colliding (Ω-like) and non-colliding (KΩ-like) waves [118, 123].

Fig. 10 illustrates the behaviour of Ω-like autowave solutions of equations (59), (60). The figure shows that autowaves generated at four points of a two-dimensional medium tend to collide on converging. This results in the formation of a cross-like static structure characterised by an increased (compared to its environment) bacterial concentration.

Fig. 11 shows the dynamics of temporal and spatial changes in bacterial density and concentration of the substrate consumed by bacteria along the line joining the sources of two converging Ω-like waves. It can be seen that at the moment of their collision the substrate concentration in this region has not yet dropped to zero, and it takes some time for this to occur.

Fig. 12 demonstrates KΩ-like dynamics of population waves obtained upon solution of equations (59), (60). Evidently, KΩ-like waves give rise to a cross-like static structure with a decreased (compared to its environment) bacterial density. Thus, spatial structures formed by KΩ-like waves are qualitatively different from those generated by the collision of Ω-like waves.

Fig. 13 shows the dynamics of b and p changes along the line connecting two sources of KΩ-like waves. It can be seen that the amplitude of the waves falls as they approach each other. This is obviously related to the formation of the demarcation zone dividing the two approaching bacterial populations; the population waves diverge in directions perpendicular to the line that connects the sources of these

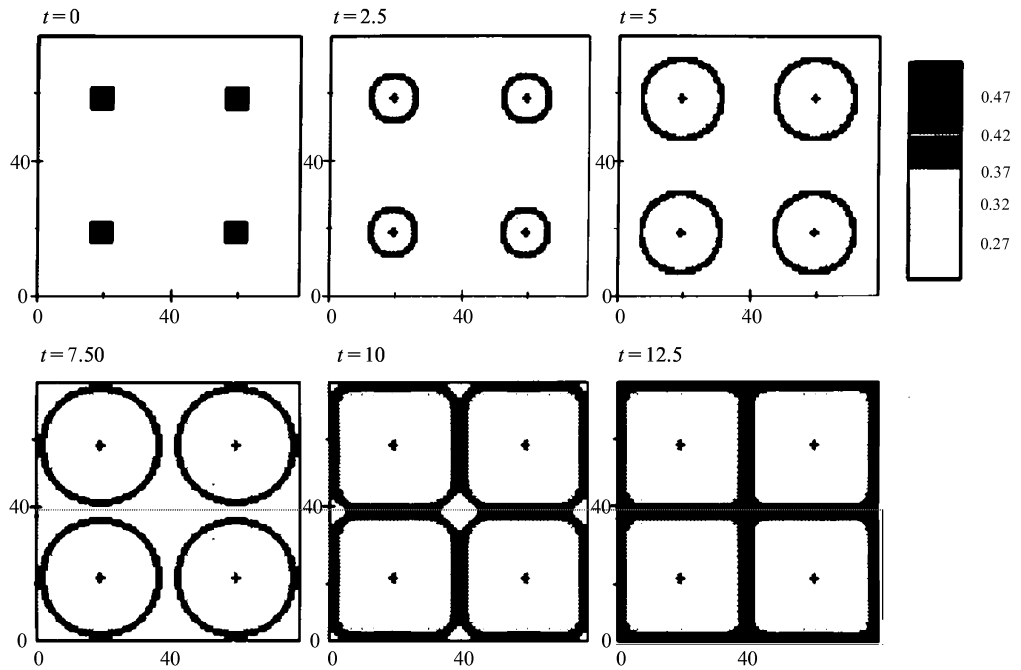

Figure 10. Formation of a cross-like static structure with enhanced bacterial density as a result of collision of Ω-like population waves [119]; the scale on the right corresponds to bacterial density.

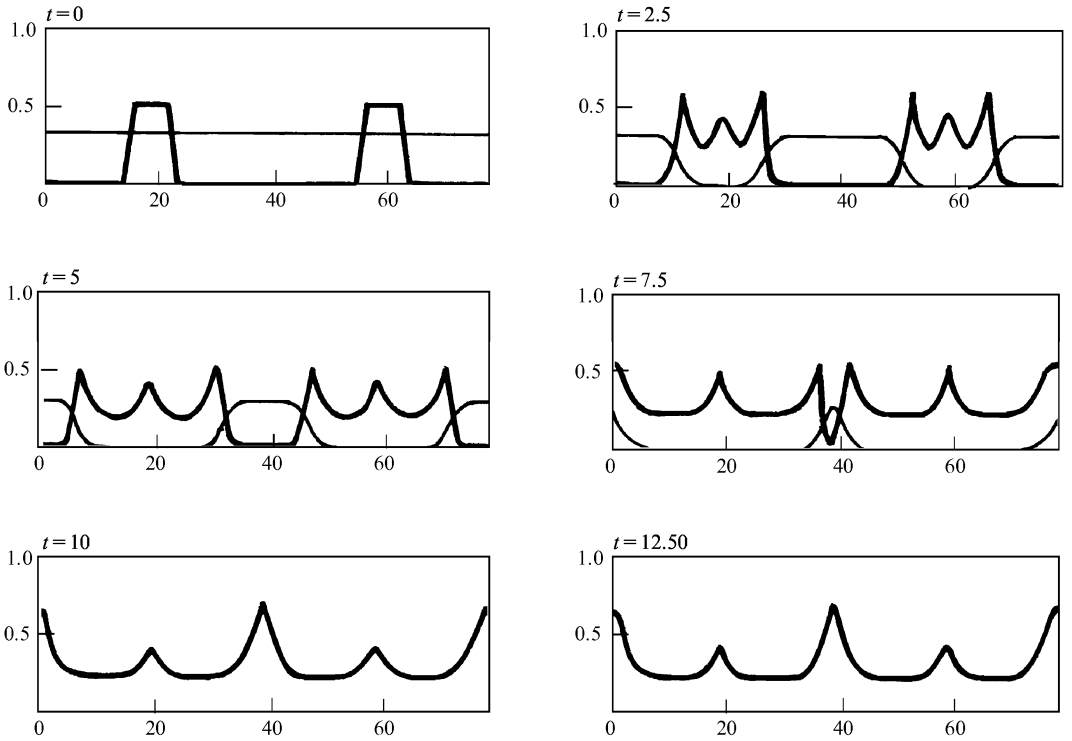

Figure 11. The dynamics of changes in bacterial density b (thick lines) and consumed substrate concentration p (thin lines) on convergence of Ω-like waves [119].

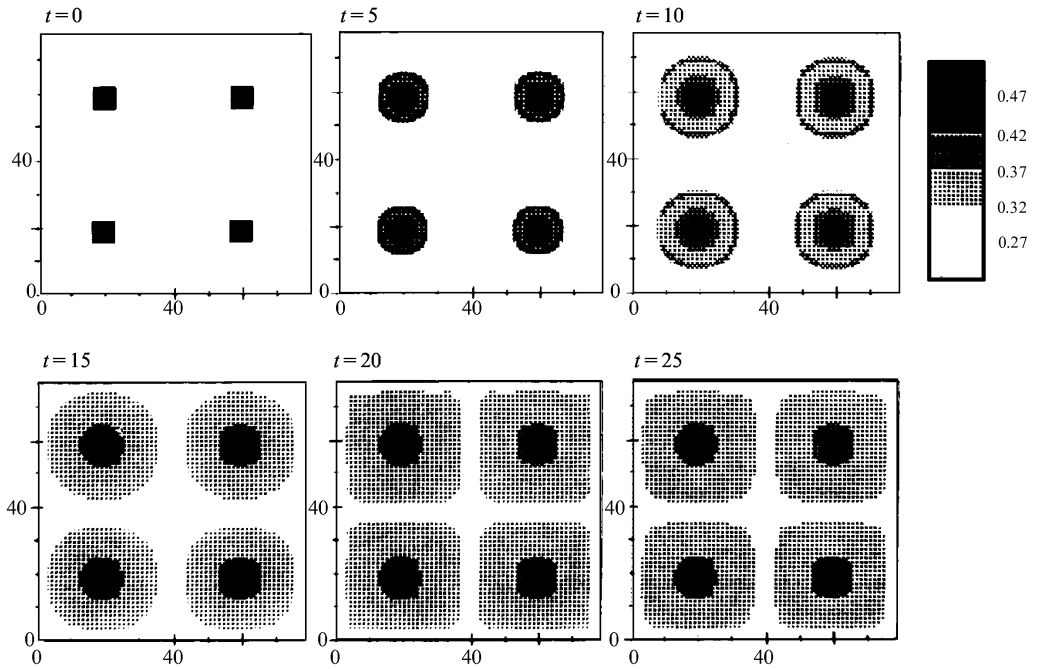

Figure 12. Formation of a cross-like static structure with decreased bacterial density on convergence of two KΩ-like bacterial waves [119]; the scale on the right corresponds to bacterial density.

waves and 'trace' the boundaries of the demarcation zone (Fig. 12).

It is seen from Fig. 13 that the demarcation zone is characterised by two conditions: (1) $b_{\text{zone}} \to 0$ and (2) $p_{\text{zone}} \to 0$. The first condition can be regarded as defining KΩ-like waves whereas the second leads to the conclusion that the formation of demarcation zones (where $p_{\text{zone}} = 0$) is due to a gradual decrease of the substrate concentration to zero as the population waves approach each other. It follows from equations (62), (63) that both motility and chemotactic response of bacteria also undergo a dramatic fall which prevents such bacterial waves from colliding.

Both Ω-like and KΩ-like waves are solutions of one and the same system of equations (59), (60). Transition from one

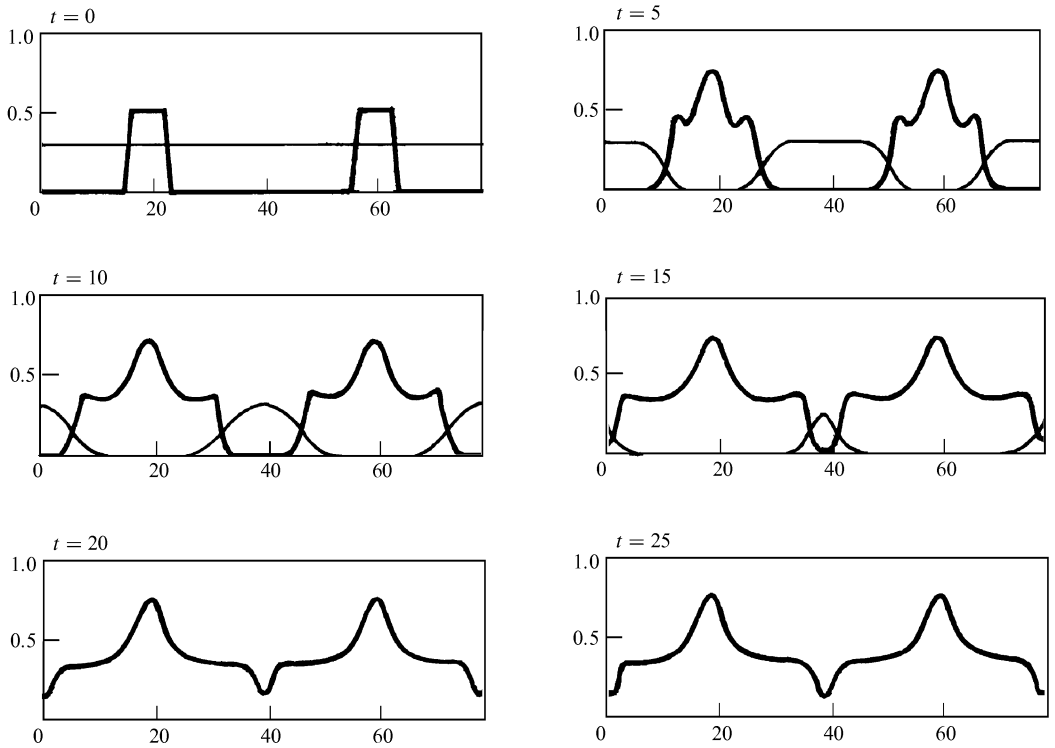

Figure 13. The dynamics of changes in bacterial density b (thick lines) and substrate concentration p (thin lines) for KΩ-like population waves [119].

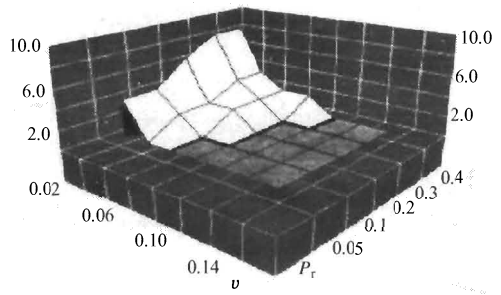

Figure 14. Dependence of the width of the demarcation zone δ (z axis) on the parameters v and P_r; $\chi(p) = 1/p$. The shaded area corresponds to the Ω regime [119].

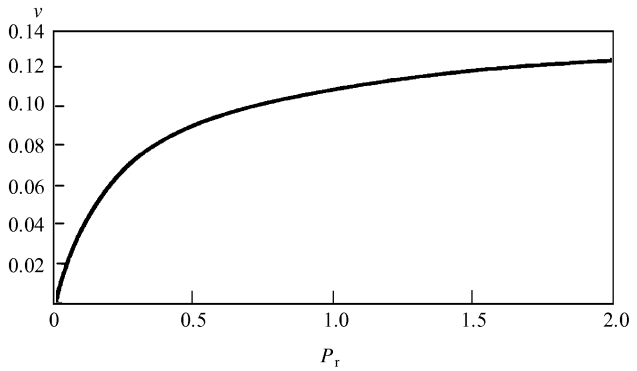

Figure 15. The boundary between Ω and KΩ regions in the (v, P_r) plane [119].

wave type to the other occurs at appropriate changes of the parameters v, P_k, and P_r on which chemotactic responsiveness of bacteria and their growth rate depend [see formulas (59), (61), and (63)].

Fig. 14 shows the dependence of the demarcation zone width δ on the parameters v and P_r, on the assumption that $\chi(p) = 1/p$ [see formula (63)]. It can be seen that δ changes from 0 (Ω-like regime) to $\cong 8.0$. Transition from the Ω-like to the KΩ-like regime of propagation of population autowaves occurs with a decrease in v and an increase in P_r, i.e. when both the chemotactic response and the bacterial reproduction rate decrease (Fig. 15).

Fig. 16 illustrates the dependence $\delta(v, P_r)$ on the assumption that $\chi(p) = P_k/(p + P_k)^2$ [see formula (63)]. Here, the transition from the Ω-like to the KΩ-like regime occurs more sharply (compare with Fig. 14).

Fig. 17 clearly demonstrates the division of the (v, P_k, P_r) space into two regions: Ω and KΩ. In the case when $\chi(p) = P_k/(p + P_k)^2$, the chemotactic response

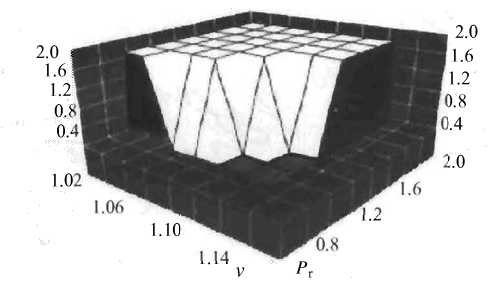

Figure 16. Dependence of the width of the demarcation zone δ (z axis) on the parameters v and P_r; $\chi(p) = P_k/(p + P_k)^2$, $P_k = 0.1$. The shaded area corresponds to the Ω regime [119].

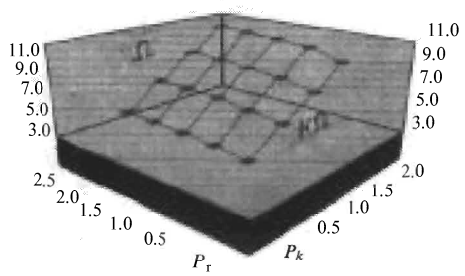

Figure 17. Two-dimensional surface separating **Ω** and K**Ω** regions in the (v, P_k, P_r) space [119].

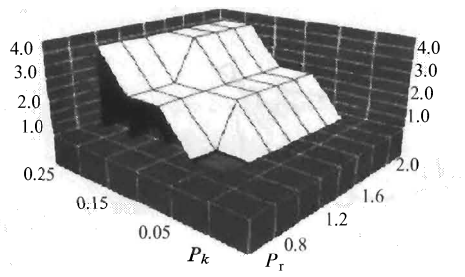

Figure 18. Dependence of the width of the demarcation zone δ (z axis) on the parameters P_k and P_r; $v = 1.1$. The shaded area corresponds to the **Ω** regime [119].

depends on two parameters (v and P_k) rather than one. In view of this, the change in the width of the demarcation zone δ as a function of the parameters P_k and P_r is of special interest. The dependence $\delta(P_k, P_r)$ is shown in Fig. 18.

It is seen from this figure that the transition from the **Ω** regime (when $\delta = 0$) to the K**Ω** regime occurs with a rise of both parameters, P_k and P_r (corresponding to a decrease in chemotactic response and bacterial growth rate).

Fig. 19 shows the dependence of the population autowave velocity U on the parameters v, P_k, and P_r for both types of functional dependences $\chi(p)$ [in accordance with formula 63)]. It can be seen that U depends weakly on the parameter P_k but increases significantly with both the growth of v and the fall of P_r. The **Ω**-like waves propagate at a higher velocity than the K**Ω**-like waves. The critical value U_{cr} at which the transition from the **Ω** region into the K**Ω** region occurs within the (v, P_k, P_r) parameter space depends on these parameters even though this dependence is not strong. All the U_{cr} values lie within a relatively narrow range of propagation velocities of population waves: 0.3–0.5 for $\chi(p) = 1/p$ and 0.2–0.3 for $\chi(P) = P_k/(p + P_k)^2$.

These findings are in good agreement with the results of our *in vivo* experiments on motile chemotactic bacteria [118, 123–125, 136, 137]. Fig. 20 shows the spatial structure which is formed when two K**Ω**-like bacterial waves approach each other in an *in vivo* experiment. It also shows changes in the nutrient substrate (glucose) concentration immediately ahead of the wave fronts and in the demarcation zone separating the two populations, in comparison with the concentration at control points located at a distance from the propagating waves. It is

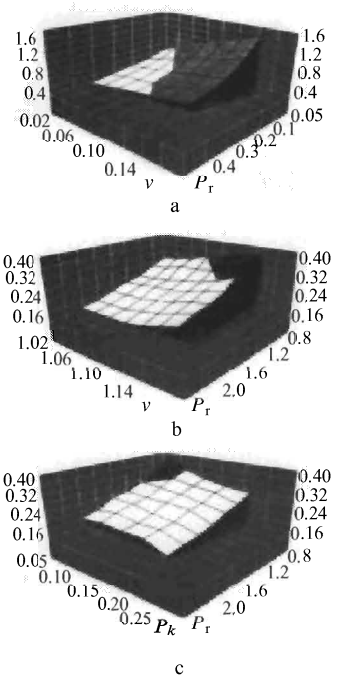

Figure 19. Dependences of the population wave velocity U (z axis) on the parameters v and P_r, $\chi(p) = 1/p$ (a); v and P_r, $\chi(p) = P_k/(p + P_k)^2$, $P_k = 0.1$ (b); P_k and P_r, $v = 1.1$ (c). The shaded area corresponds to the **Ω** regime [119].

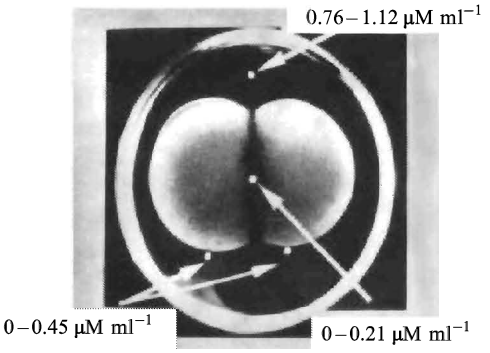

Figure 20. The decrease of glucose concentration in the agar nutrient medium when a demarcation zone is formed. The glucose sampling points shown are as follows: at a distance from the converging waves (control), immediately ahead of the wave fronts, and in the demarcation zone [119, 138].

clearly seen that the glucose concentration decreases significantly ahead of the wave fronts and even more so within the demarcation zone. Table 2 contains more detailed information obtained in these experiments. It also shows that the fall in glucose concentration in the demarcation zone (0 – 21% of the control value) is, on average, more pronounced than ahead of the population wave fronts (0 – 45% of the control values).

These results obtained by biochemical methods have been confirmed in experiments in which radioisotope tracers were used [123, 136, 138].

Interestingly, glucose concentrations on both sides of the demarcation zone boundary were nearly identical, so that the ratio of these concentrations in our experiments did not exceed 2. However, the chemotactic response of *E. coli*

Table 2. Glucose concentration changes when two KΩ-like bacterial population waves approach each other.

Sampling points	Glucose concentration/mM				
	Experiment 1	Experiment 2	Experiment 3	Experiment 4	Experiment 5
Control	1.12 ± 0.2	0.76 ± 0.13	0.87 ± 0.08	0.96 ± 0.14	1.00 ± 0.1
Ahead of wave fronts	0.14 ± 0.33	0.22 ± 0.01	0	0.25 ± 0.01	0.45 ± 0.02
In the demarcation zone	0.11 ± 0.01	0.16 ± 0.01	0	0.09 ± 0.01	0.21 ± 0.06

to sugars is known to occur only when this ratio is close to 100 [103].

Therefore, the fall in glucose concentration appears to be the determining factor in the formation of demarcation zones. A similar effect was observed in computer simulations (Fig. 13). It is important to note that in accordance with the results of computer simulations, the transition from KΩ-like waves to Ω-like ones *in vivo* was characterised by an increase in the wave propagation velocity to a certain critical value (ca. 4 mm h^{-1}) [124].

The question arises: why the demarcation zones do not dissipate 10 or even more hours after their formation, as has been shown in our earlier studies? Evidently, this can be attributed to the decrease in substrate concentration in the demarcation zone below a certain critical level resulting in a markedly reduced bacterial motility [in compliance with formula (62)]. In computer simulations, demarcation zones did not form when this condition was not fulfilled [123].

To summarise, extensive experimental studies have demonstrated that spatial structures formed by motile bacteria can be very unstable (e.g. local clusters of bacteria form around inoculation points in bacterial cultures) [13, 31, 35, 93, 96, 101, 103, 119, 137]. Instability of such structures (their schematic representation is given in Fig. 21A) may be caused by continuous changes of the nutrient substrate distribution (owing to its consumption by bacteria) and also by bacterial motility and chemotaxis. Unstable structures are eventually transformed into other, more stable ones. The transformation patterns depend on both the properties of bacteria and the parameters of the nutrient medium. The two types of structures thus formed are shown in Figs 21B and 21C (compare with Figs 7 and 8). It is interesting that the spatial structure presented in Fig. 21B appears, in its turn, to be unstable under certain conditions (e.g. when the bacteria forming population waves in a multi-component nutrient medium can switch from preferable consumption of one substrate assortment to the consumption of another); this may result in the formation of a structure resembling the one shown in Fig. 21C [13, 121–124]. The transition A → B (Fig. 21) is produced by rapid Ω-like waves (propagating at velocities exceeding the critical value), whereas the transition A → C is accomplished by slow KΩ-like waves. In the latter case a demarcation zone separating individual cell populations is formed (Figs 8, 12, 20).

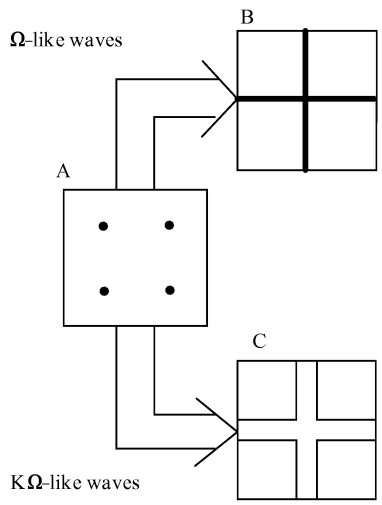

Figure 21. Autowave transformation of unstable bacterial clusters into two types of spatial structures [119].

3.2 TM waves

It is noteworthy that in addition to the above two regimes of bacterial wave interaction, a third type has recently been described [139]. It has been found that superfast bacterial waves (propagation velocities in excess of 9 mm h^{-1}) approaching each other behave like solitons (i.e. in a way very unusual for autowaves). They appear to be reciprocally permeable and neither interfere with each other nor change their velocity during their interaction. Such mode of interaction is called the TM regime and the corresponding waves are referred to as TM waves [139].

The soliton-like behaviour of TM waves is illustrated in Fig. 22. A possible mechanism responsible for the induction of the TM regime was investigated in numerical simulation based on mathematical model (59)–(63) [139]. It was found that propagating TM-waves leave behind them a certain amount of substrate unmetabolised by bacterial cells and sufficient for a gradient to form in the region where TM wave fronts collide and bacterial density is enhanced. As a result, the collision may be followed by further propagation of individual TM waves without the bacteria switching to the consumption of another substrate (in contrast to the situation observed in the case of Ω-like population waves [13, 118]), until the concentration of the consumed substrate just ahead of the TM waves falls to zero owing to its utilisation by bacterial cells which have remained behind and did not participate in the population TM waves [139].

It is known that autowaves play an active role in the morphogenesis of multicellular organisms. They may also include waves of mechanical activity of epithelial cells [140], calcium waves generated upon egg-cell fertilisation [141], waves arising from cell aggregation in *Dictyostelium discoideum*, and also wave processes associated with the developmental stages of this slug following aggregation [13, 142–144]. Autowave involvement in the above processes may account for the growing drive to discover new types of autowaves (e.g. TM autowaves) and for studies of the interaction between autowaves (with memory and without it) and their role (along with that

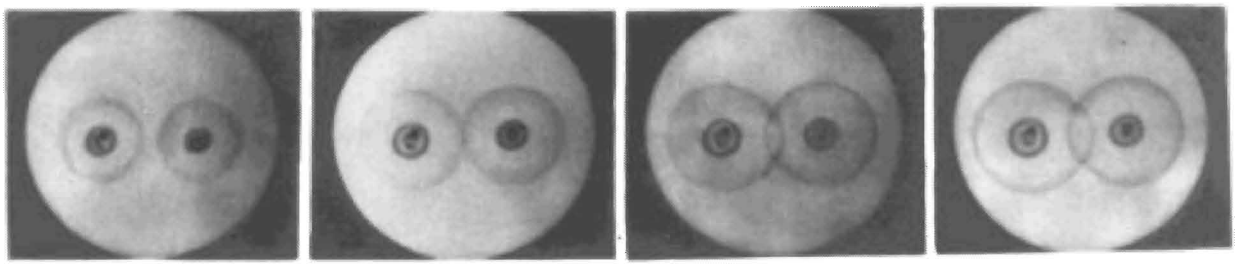

Figure 22. Soliton-like behaviour of two bacterial population autowaves (TM waves) approaching each other [139].

of the Turing mechanism [77, 81, 82, 87, 131, 135, 145]) in the formation of biological structures.

4. Unstable propagation regimes of population waves formed by motile chemotactic cells

4.1 Stability of classical autowaves formed by elements devoid of memory

Stability of autowaves is a cardinal problem in the physics of excitable media [123]. In the early 1940s, Kokochashvili was the first to show impaired stability of flame propagation front in a hydrogen/bromine mixture (35% – 40% H_2 and 60% – 65% Br_2) [146, 147]. The theory of this phenomenon was worked out by Zel'dovich [147]. The stability (or instability) of the flame front was found to be dependent on the ratio of the coefficient of diffusion to thermal conductivity. In mixtures in which the coefficient of diffusion exceeds thermal conductivity, increased fuel supply due to diffusion in a randomly formed convex front zone prevails over loss of heat from the unburnt portion of the mixture; this results in a higher combustion rate. Conversely, in a mixture with a concave front the loss of fuel through diffusion prevails over heat generation which accounts for a decreased combustion rate and instability of the plane autowave [147].

Later, Kuramoto [148 – 151] undertook a more detailed theoretical analysis of autowave stability in re-excitable and non-reexcitable media. He demonstrated that the autowave front may lose stability when the diffusion coefficient of the inhibitor exceeds the diffusion coefficient of the activator, assuming that the front is formed by elements devoid of memory and can therefore be described by typical autowave 'reaction – diffusion' equations. In vector form, these equations can be written as:

$$\frac{\partial \boldsymbol{X}}{\partial t} = D\left(\frac{\partial^2}{\partial x^2} + \frac{\partial^2}{\partial y^2}\right)\boldsymbol{X} + F(\boldsymbol{X}) , \tag{64}$$

where $\boldsymbol{X} = (X_1, X_2, \ldots, X_n)$ is a vector with concentration variables serving as its coordinates and D is the diagonal diffusion matrix. In order to examine the stability of the autowave described by equation (64) by the conventional approach, it is necessary to specify a small spatial deformation of the wave front similar to that depicted in Fig. 23. The weak dependence of $\boldsymbol{X}$ on the coordinate y can be formally presented as:

$$\frac{\partial \boldsymbol{X}}{\partial t} = F(\boldsymbol{X}) + D\frac{\partial^2 \boldsymbol{X}}{\partial x^2} + \varepsilon \boldsymbol{p} ,$$

$$\boldsymbol{p} = D\frac{\partial^2 \boldsymbol{X}}{\partial y^2} . \tag{65}$$

By analogy with perturbation of a one-dimensional system according to

$$\boldsymbol{X}(z,t) = \boldsymbol{X}_0 + \boldsymbol{u}(z,t) ,$$

where $z = x - c(t + \psi_0)$ and c is the front velocity, two-dimensional perturbation of the autowave front was simulated by the equation [150, 152]:

$$\boldsymbol{X}(x,y,t) = \boldsymbol{X}(\xi,[\Phi]) \equiv \boldsymbol{X}_0(\xi) + \boldsymbol{u}(\xi,[\Phi]) , \tag{66}$$

where

$$\xi = x - c\Phi(y,t) , \tag{67}$$

$$\boldsymbol{X}(\xi,[\Phi]) \equiv \boldsymbol{X}\left(\xi, \sqrt{\varepsilon}\frac{\partial \Phi}{\partial y}, \varepsilon\frac{\partial^2 \Phi}{\partial y^2}, \ldots\right) , \tag{68}$$

$$\boldsymbol{u}(\xi,[\Phi]) \equiv \boldsymbol{u}\left(\xi, \sqrt{\varepsilon}\frac{\partial \Phi}{\partial y}, \varepsilon\frac{\partial^2 \Phi}{\partial y^2}, \ldots\right) . \tag{68a}$$

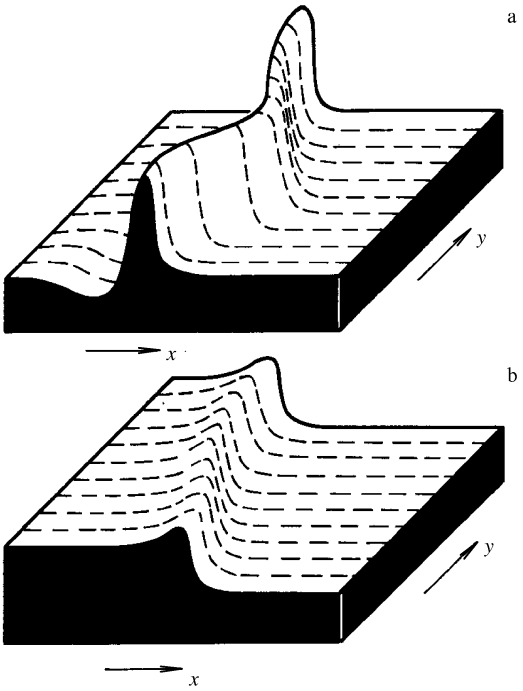

Figure 23. Distortion of wave fronts: (a) impulse-like and (b) switching wave [151].

In equation (67), $\Phi(y,t)$ is a function changing slowly with y which is reflected in the small factor ε. The shape of this function is defined by the following equation [151]:

$$\frac{\partial \Phi}{\partial t} = 1 + \Omega[\Phi] , \tag{69}$$

where

$$\Omega[\Phi] \equiv \Omega\left(\sqrt{\varepsilon}\frac{\partial \Phi}{\partial y}, \varepsilon\frac{\partial^2 \Phi}{\partial y^2}, \ldots\right) .$$

The form of the function $\Omega[\Phi]$ may be determined by substitution of expression (66) [with account taken of identity (68) and equation (69)] into equation (65) followed by expansion into powers of ε:

$$\Omega[\Phi] = \sum_{\nu=1}^{\infty} \varepsilon^{\nu} \Omega_{\nu}[\Phi] , \tag{70}$$

where [152]

$$\Omega_1[\Phi] = \alpha\frac{\partial^2 \Phi}{\partial y^2} + \beta\left(\frac{\partial \Phi}{\partial y}\right)^2 , \tag{71}$$

$$\Omega_2[\Phi] = -\gamma\frac{\partial^4 \Phi}{\partial y^4} + \ldots + \delta\left(\frac{\partial \Phi}{\partial y}\right)^4 \tag{72}$$

etc. The coefficients α, β, γ (the coefficient δ will not be needed below) are defined as [151]:

$$\alpha \equiv (0|D|0) , \tag{73a}$$

$$\beta \equiv -c\left(0\left|D\frac{\mathrm{d}}{\mathrm{d}\xi}\right|0\right) , \tag{73b}$$

$$\gamma \equiv \sum_{l\neq 0} \lambda_l^{-1} (0|D|l)(l|D|0) , \tag{73c}$$

with the following notation:

$$(l|A|m) \equiv \int_{-\infty}^{\infty} \boldsymbol{u}_l^*(\xi) A \boldsymbol{u}_m(\xi)\,\mathrm{d}\xi . \tag{74}$$

In formulas (73) and (74), λ_l and $\boldsymbol{u}_l$ $(l = 0, 1, 2, \ldots)$ are the eigenvalues and the corresponding eigenvectors of the operator

$$\Gamma(z) = L(z) + c\frac{\mathrm{d}}{\mathrm{d}z} + D\frac{\mathrm{d}^2}{\mathrm{d}z^2} . \tag{75}$$

In equation (75), $L(z)$ is a Jacobian in which the ij-th element is $\partial F_i(\boldsymbol{x}_0)/\partial \boldsymbol{x}_{0j}$, and $\boldsymbol{u}_l^*$ in (74) is the eigenvector of the operator

$$\Gamma^*(z) = {}^{\mathrm{t}}L(z) - c\frac{\mathrm{d}}{\mathrm{d}z} + {}^{\mathrm{t}}D\frac{\mathrm{d}^2}{\mathrm{d}z^2} , \tag{76}$$

corresponding to the eigenvalue λ_l, where the index t stands for transposition. The eigenvectors are orthonormalised as follows:

$$\int_{-\infty}^{\infty} \boldsymbol{u}_l^*(z)\boldsymbol{u}_m(z)\,\mathrm{d}z = \delta_{lm} ,$$

where δ_{lm} is the Kronecker delta. It is assumed that $\boldsymbol{u}_0(z) = \mathrm{d}\boldsymbol{X}_0/\mathrm{d}z$.

Taking into account expressions (70)–(76), one can transform the evolution equation (69) to [149, 151]

$$\frac{\partial \psi}{\partial t} = \alpha\frac{\partial^2 \psi}{\partial y^2} + \beta\left(\frac{\partial \psi}{\partial y}\right)^2 - j\frac{\partial^4 \psi}{\partial y^4} + \ldots , \tag{77}$$

where $\Psi = \Phi - t$. Neglecting all terms in the right-hand side of equation (77) except the first two and substituting [152]:

$$\psi = \frac{\alpha}{\beta}\ln U , \qquad y = \frac{\alpha}{\beta}u ,$$

we can transform the 'truncated' evolution equation to

$$\frac{\partial U}{\partial t} = \frac{\beta^2}{\alpha}\frac{\partial^2 U}{\partial u^2} . \tag{78}$$

The form of equation (78) coincides with that of the diffusion equation and the ratio β^2/α corresponds to the diffusion coefficient. It is clear that, at $\alpha < 0$, solutions of the evolution equation become unstable. The question arises whether α takes on a negative value. Using the specific model

$$\frac{\partial x}{\partial t} = -X + H(X - a) - Y + D_{\mathrm{X}}\Delta X ,$$

$$\frac{\partial Y}{\partial t} = bX - cY + D_{\mathrm{Y}}\Delta Y , \tag{79}$$

where $H(X-a)$ is the Heaviside's function, Kuramoto [149, 151] showed that α is determined by the formula:

$$\alpha = \sqrt{\varepsilon}\widetilde{D}_{\mathrm{X}}\left[1 - \frac{\widetilde{b}}{(1-2a)^2}\left(\frac{D_{\mathrm{Y}}}{\widetilde{D}_{\mathrm{X}}}\right)^2\right] \tag{80}$$

and can take on negative values. In equations (79) and (80), a, b, D_{X}, and D_{Y} are non-negative parameters of the model, and ε is a parameter determining the smallness of the quantities b, c, and D_{X}:

$$b = \varepsilon\widetilde{b} ,$$

$$c = \varepsilon\widetilde{c} ,$$

$$D_{\mathrm{X}} = \sqrt{\varepsilon}\widetilde{D}_{\mathrm{X}} .$$

According to formula (80), the transition from positive to negative values of α occurs during motion in the parameter space, e.g. when the diffusion coefficient D_{Y} of the 'inhibitor' Y increases. Taking into account higher order terms one cannot rule out that unstable regimes will not arise [148, 151, 153, 154].

To obtain a better insight into the mechanism of their formation, consider a bistable system consisting of an activator X and an inhibitor Y. Assume that the entire medium is divided by the autowave front into two regions as shown in Fig. 24a and that each region corresponds to its stable state: (X_1, Y_1) and (X_2, Y_2). Also, assume that $X_1 > X_2$ and hence $Y_1 > Y_2$.

Let us suppose that an initially plane wave front has suffered a small perturbation (Fig. 24b) and examine its evolution. For autowave instability (as well as for the Turing structures [145]) to occur, it is necessary that the diffusion rate of Y should be higher than that of X [147, 149, 151, 155]. Because of this, the isoconcentration contour of Y looks and actually is somewhat smoother than the front of X (Fig. 24b). As a result, the most convex part of the front of X (designated as A in Fig. 24b) is located in the region with reduced Y concentration. At the same time, the concave parts of the front of X (indicated by letters B and C in Fig. 24b) coincide with the region of enhanced levels of Y

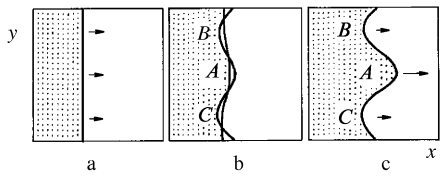

Figure 24. Mechanism of autowave front instability [152].

(Fig. 24b). The deficit of Y facilitates the production of X; conversely, the production of X is inhibited by increased Y concentrations. When these effects are sufficiently strong to counterbalance the smoothing effect of diffusion, they may become capable of amplifying the originally weak perturbation of the shape of the autowave front leading to the development of diffusional instability (Fig. 24c).

Another interesting mechanism of autowave instability is inherent in bistable anisotropic active media whose diffusion properties do not change along any particular direction but are different for different directions. Such an instability was investigated by Mornev [156].

Anisotropic active media are characterised by diffusion coefficients having a tensor nature. For this reason, instead of the equation describing mass transfer due to diffusion

$$\boldsymbol{J} = -D\vec{\nabla}u \ ,$$

where u is the concentration variable, the following equation applies:

$$\boldsymbol{J} = -\widehat{D}\vec{\nabla}u \ , \tag{81}$$

where $\widehat{D}$ is a linear operator performing the rotation of vectors $\boldsymbol{y}$ and $\vec{\nabla}u$ relative to each other (diffusional anisotropy effect). It is possible to rewrite equation (81) as follows

$$J_\alpha = -D_{\alpha\beta}\frac{\partial u}{\partial x_\beta} \ , \tag{82}$$

where the summation is performed over repeated indices β. In equations (81) and (82), $\widehat{D}$ is the diffusion tensor of the excitable (active) medium defined in each spatial coordinate system by corresponding matrices of its components $[D_{\alpha\beta}]$ and J_α are the components of $\boldsymbol{J}$ in the same coordinate system.

The tensor $\widehat{D}$ in equation (81) must fulfill the following two conditions:

(i) it must be nondegenerate, i.e.

$$\det [D_{\alpha\beta}] \neq 0 \ ;$$

(ii) all eigenvalues of $\widehat{D}$ must be positive.

Condition (i) ensues from the one-to-one relationship between $\boldsymbol{J}$ and $\vec{\nabla}u$. This automatically leads to the existence of a complete set of nonvanishing eigenvalues $D_1, D_2, \ldots$, of tensor $\widehat{D}$ and corresponding principal axes defined by unit linearly independent eigenvectors $\boldsymbol{a}_1, \boldsymbol{a}_2, \ldots$.

Condition (ii) follows from the physical meaning of the eigenvalues $D_1, D_2, \ldots$ of tensor $\widehat{D}$: D_k is the diffusion coefficient in the case when $\vec{\nabla}u$ is located on the k-th principal axis of tensor $\widehat{D}$. It is clear that a diffusion coefficient cannot be negative.

For an anisotropic medium, equation (6) takes on the form:

$$\frac{\partial u}{\partial t} = D_{\alpha\beta}\frac{\partial^2 u}{\partial x_\alpha \partial x_\beta} + f(u) \ . \tag{83}$$

In equation (83), summation is performed over repeated indices.

The presence of anisotropy of an active medium, described by equation (83), accounts for the dependence of the steady-state velocity a of the plane wave travelling in such a medium on the direction $\vec{n}$ in which it propagates: $v = v(\boldsymbol{n})$.

In the case of a symmetric tensor $\widehat{D}$ ($D_{\alpha\beta} = D_{\beta\alpha}$), that is when the principal axes of $\widehat{D}$ are mutually orthogonal, the dependence of velocity on direction is relatively simple. Thus the velocity V_k of a switching autowave propagating along the k-th principal axis is proportional to $\sqrt{D_k}$, where D_k is the k-th eigenvalue of tensor $\widehat{D}$. Such a medium has been examined in detail in connection with the analysis of excitation wave propagation in anisotropic neuromuscular syncytia in which electric conductivity played the role of the diffusion tensor [157].

When $D_{\alpha\beta} \neq D_{\beta\alpha}$, the two principal axes of tensor $\widehat{D}$ are not mutually orthogonal and the minimum adjacent angle θ between them (the so-called 'angle of anisotropy' [156]) serves as a parameter that markedly affects autowave propagation patterns. It has been demonstrated [156] that in this case the autowave velocity depends both on the direction of its propagation and on the parameters of anisotropy defined by tensor $\widehat{D}$. This dependence is described by the formula [156]:

$$a = \alpha(\boldsymbol{n})a_e \ , \tag{84}$$

where

$$\alpha(\boldsymbol{n}) = \sqrt{\widehat{D} : \widehat{n}^2} \ . \tag{85}$$

In formula (84), a_e is the velocity of a plane autowave in a reference isotropic medium (with $D = 1$) and with the same function $f(u)$ as in the anisotropic medium [the reference isotropic medium is described by equation (6) while the anisotropic one is characterised by equation (83)]. In formula (85), $\alpha(\boldsymbol{n})$ is the absolute autowave refractive index of the anisotropic medium in direction $\boldsymbol{n}$ and the expression under the root sign is a double convolution of tensor $\widehat{D} \equiv [D_{\alpha\beta}]$ and tensor $\widehat{n}^2 \equiv [n_\mu n_\nu]$, i.e.

$$\widehat{D} : \widehat{n}^2 = D_{\alpha\beta}n_\alpha n_\beta \ . \tag{86}$$

In expression (86), the summation is performed over repeated indices.

Expressions (84)–(86) have been obtained by the following simple line of reasoning. Suppose that

$$u = u_e(\tau) \ ,$$

$$\tau = t - \boldsymbol{n}\cdot\boldsymbol{x}a_e^{-1} \ ,$$

$$\boldsymbol{n}\cdot\boldsymbol{x} = n_\alpha x_\alpha \ ,$$

$$n^2 = n_1^2 + n_2^2 + \ldots = 1 \tag{87}$$

is a self-modelling solution of equation (6) with $D = 1$. Such a solution is known to correspond to a switching wave that propagates in an isotropic ('reference') medium with a velocity a_e in direction $\boldsymbol{n}$. Substitution of expression (87) into equation (6) (at $D = 1$) yields the following differential equation:

$$\kappa\frac{d^2u_e}{d\tau^2} - \frac{du_e}{d\tau} + f(u_e) = 0 \ , \tag{88}$$

where

$$\kappa = \frac{1}{a_e^2} . \qquad (89)$$

Equation (88) fulfills boundary conditions which define two stable states of the active medium for a switching wave at $\tau \to \pm\infty$. These conditions being fixed, the value of parameter κ, which is the eigenvalue of the boundary problem and is defined by equality (89), can be uniquely and unambiguously determined. This yields the velocity $a_e = \kappa^{-1/2}$.

Now, consider the self-modelling solution

$$u = u(\tau) ,$$
$$\tau = t - \boldsymbol{n}\cdot\boldsymbol{x}a^{-1} ,$$
$$\boldsymbol{n}\cdot\boldsymbol{x} = \boldsymbol{n}_\alpha\cdot\boldsymbol{x}_\alpha ,$$
$$n^2 = n_1^2 + n_2^2 + \ldots = 1 \qquad (90)$$

of equation (83) which describes a switching autowave spreading in direction $\boldsymbol{n}$ in an anisotropic bistable medium. Substitution of expression (90) into equation (83) leads to a boundary problem which includes the equation:

$$\kappa\frac{d^2u}{d\tau^2} - \frac{du}{d\tau} + f(u) = 0 , \qquad (91)$$

where

$$\kappa = \frac{D_{\alpha\beta}n_\alpha n_\beta}{a^2} . \qquad (92)$$

It is obvious that equation (91) coincides with equation (88). In both problems, the parameter κ has the same value if we assume that the boundary conditions of equations (88) and (91) also coincide. Equating expressions (89) and (92) we find that

$$a \equiv a(\boldsymbol{n}) = a_e\sqrt{D_{\alpha\beta}n_\alpha n_\beta} = a_e\sqrt{\widehat{D} : \widehat{n}^2} , \qquad (93)$$

which proves formula (84), with equalities (85) and (86) taken into account.

An important corrolary of equation (93) is that plane autowave propagation is impossible along directions $\boldsymbol{n}$ (the so-called 'autowave opacity directions' or 'forbidden directions of propagation' [156]) for which the following inequality holds:

$$\alpha^2(\boldsymbol{n}) = (\widehat{D} : \widehat{n}^2) \leqslant 0 . \qquad (94)$$

In fact, the refractive index [defined by formula (85)] along autowave opacity directions either equals 0 [when the right-hand side of equation (94) is zero] or is purely imaginary [when inequality (94) is strictly fulfilled]. Accordingly, the velocity a defined by formula (84) and proportional to $\alpha(\boldsymbol{n})$ is also equal to zero or purely imaginary for these directions. This implies that, for the forbidden directions $\boldsymbol{n}$, equation (83) does not have autowave solutions in the form of switching waves travelling with a real nonvanishing velocity a.

It has been shown [156] that the quantity $\alpha^2(\boldsymbol{n}) = \widehat{D} : \widehat{n}^2$ can be determined in the following way:

$$\alpha^2(\varphi) = A + B(\theta)\sin 2\varphi . \qquad (95)$$

In equation (95), θ is the angle of anisotropy, and φ is the angle between direction $\boldsymbol{n}$ and the axis of abscissae,

$$A = \frac{1}{2}(D_2 + D_1) , \quad B = \frac{1}{2\sin\theta}(D_2 - D_1) ,$$

$D_1 > 0$ and $D_2 > 0$ are eigenvalues of tensor $\widehat{D}$. It follows from equation (95) that autowave opacity directions fulfill the inequality:

$$A + B(\theta)\sin 2\varphi \geqslant 0 . \qquad (96)$$

Inequality (96) corresponds to angles of anisotropy θ for which the plot of function $\alpha^2(\varphi)$ touches the axis of abscissae or intersects it. The analytical condition for the emergence of opacity sectors has the form [156]:

$$\theta < \arcsin\frac{D_2 - D_1}{D_2 + D_1} .$$

What is the underlying physical reason behind the appearance of forbidden directions? To answer this question we shall examine the relationship between the geometry of the disposition of vectors $\boldsymbol{J}$ and $\vec{\nabla}$ and the autowave refractive index α. $\boldsymbol{J}$ may be represented as the sum:

$$\boldsymbol{J} = \boldsymbol{J}_\parallel + \boldsymbol{J}_\perp ,$$

where $\boldsymbol{J}_\parallel$ lies on the same straight line as $\vec{\nabla}u$ while $\boldsymbol{J}_\perp$ is perpendicular to it. Since

$$\boldsymbol{J}_\parallel = (\boldsymbol{J}_\parallel\cdot\boldsymbol{q})\boldsymbol{q} \cong J_\alpha q_\alpha \boldsymbol{q} ,$$

where $\boldsymbol{q}$ is a unit vector codirectional with $\vec{\nabla}u$ and q_α are direction cosines of $\boldsymbol{q}$, it follows [on taking into account equation (82)] that:

$$\boldsymbol{J}_\parallel = -D_{\alpha\beta}q_\alpha\frac{\partial u}{\partial x_\beta}\boldsymbol{q} . \qquad (97)$$

Note that

$$\frac{\partial u}{\partial x_\beta} = |\vec{\nabla}u|q_\beta .$$

Owing to this, equation (97) assumes the form

$$\boldsymbol{J}_\parallel = -D_{\alpha\beta}q_\alpha q_\beta|\vec{\nabla}u|\boldsymbol{q} = -(\widehat{D} : \widehat{q}^2)\vec{\nabla}u .$$

From this and equation (85) it follows that

$$\boldsymbol{J}_\parallel = -\alpha^2(\boldsymbol{q})\vec{\nabla}u . \qquad (98)$$

It is clear from equation (98) that $\boldsymbol{J}_\parallel$ is directed against the gradient u when and only when $\alpha^2(\boldsymbol{q}) > 0$. Conversely, if $\alpha^2(\boldsymbol{q}) = 0$, then $\boldsymbol{J}_\parallel$ is orthogonal to $\vec{\nabla}u$. Finally, when $\alpha^2(\boldsymbol{q}) < 0$, i.e. when the refractive index $\alpha(\boldsymbol{q})$ in the $\boldsymbol{q}$ direction has an imaginary value, then $\boldsymbol{J}_\parallel$ is codirectional with $\nabla\vec{u}$. This means that if $\vec{\nabla}u$ coincides with one of the directions lying in opacity sectors, the medium contains a component of activator flow which is described by vector $\boldsymbol{J}_\parallel$ and is coincident with the direction in which its concentration grows. This makes it impossible for autowaves to propagate along directions corresponding to imaginary or zero values of $\alpha(\boldsymbol{q})$.

Hence, the inevitable loss of stability and disintegration into fragments of any plane autowave front the normal to which lies in the opacity sector. It should be noted, however, that the author of this model [156] himself questions the possibility of the existence of active media having a diffusion tensor with non-orthogonal eigenvectors.

4.2 Spontaneous bursting of the symmetry of population autowaves formed by mobile microorganisms possessing chemotaxis

Unlike classical autowaves, population waves are often formed by 'particles' (individuals) posessing memory and taxis. It is therefore tempting to suggest that this difference

may account not only for the specific features of population wave propagation and interaction but also for the possible disturbance of spatial structures generated by these waves. This subsection is largely dedicated to the examination of the distortion of symmetry of such autowave patterns.

Usually, inoculation of bacterial cells at some point of semisolid (agar) nutrient medium is almost immediately followed by their reproduction and formation of a round spot that expands from the inoculation point, representing bacterial growth. This parent bacterial population produces spreading concentric circles of population waves [93] (Fig. 25a). The mechanism of this process has been examined in detail [101] and shown to involve release of bacterial population waves, one after another, when chemotaxis effects prevail over effects associated with cell motility.

The symmetry of autowave patterns is subject to spontaneous disturbance upon a rise in agar density [13, 91, 123, 159]. This was reported to be the case when agar concentration was increased to 0.3% or higher (provided this did not interfere with the motility of bacterial cells). Such an increase resulted in the parent bacterial population giving rise to randomly distributed arch-shaped waves ('bursts') rather than to regular concentric structures [13, 91, 123, 159] (Fig. 25b).

What is the mechanism of transition from symmetric (Fig. 25a) to asymmetric wave patterns? One possibility was predicted by computer simulation.

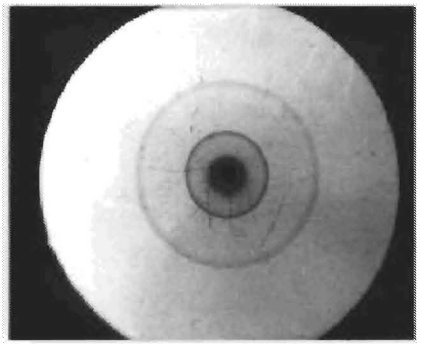

a

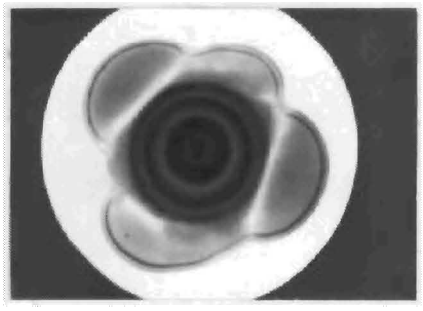

b

Figure 25. (a) Typical symmetric wave patterns formed by chemotactic bacteria *E. coli* in semisolid nutrient medium; agar concentration 0.28%. (b) Typical asymmetric wave patterns formed by chemotactic bacteria *E. coli* in semisolid nutrient medium; agar concentration 0.34%. Each burst shows two waves following each other in succession [118, 24, 158].

The mathematical model designed to answer the above question [123] describes the motion of zero-size 'cells' in an attractant concentration field in accordance with the 'chemotactic behaviour codex'. Any such 'cell' is an independent entity travelling with constant speed (v) during time (T) in the direction determined by angle ϑ.

After a lapse of time T, angle ϑ undergoes random changes within the interval $[0, 2\pi]$. As in the case of live bacterial cultures, time T in the model depends on the attractant level, that is T increases by the amount T_1 at the instant $t+\tau$ (where τ is the time step) 'the cell' reaches a point with attractant concentration exceeding that in the previous point of the space at the previous instant t (the 'cell memory' effect). The constant T_1 is the parameter of the model.

The concentration field consists of $K_x \times M_y$ squares. Attractant concentration (C_0) in any given square at instant $t+\tau$ depends on the attractant level in N adjoining squares at instant t (diffusion effect). This dependence is described by the formula:

$$C_0(t+\tau) = \left[\sum_n C_n(t) + DC_0(t)\right](D+n)^{-1}\,, \qquad (99)$$

where D is a constant. If, for instance, $D=1$, $n=8$, $C_0(t)=9$, $C_n(t)=0$ $(n=1,2,3,\ldots,8)$, then it follows from expression (99) that $C_0(t+\tau)=1$ (Fig. 26). At $C_0 \leqslant C_{\min}$ ($C_{\min}$ is the parameter of the model), the velocity of the 'cell' falls in accordance with the parabolic law. Therefore, at attractant concentrations below the threshold value, the 'cell' loses motility [in model (59), (60) this phenomenon was taken into account by formula (62)].

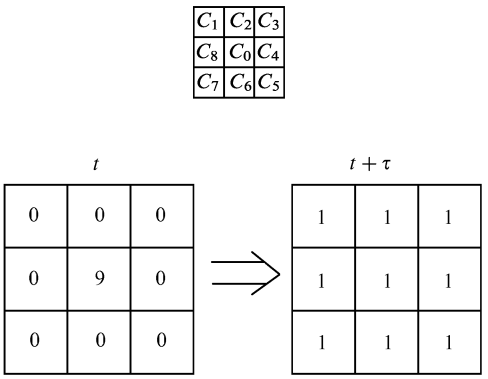

Figure 26. Attractant difusion in compliance with formula (99).

In addition to the aforementioned 'chemotactic behaviour codex', it is assumed that the 'cells' are capable of reproduction. Reproduction of an individual 'cell' is characterised by quantities τ_{cell} which at the outset are randomly distributed among 'cells' within the interval $[0, \tau_{\max}]$, where $\tau_{\max}$ is the lifespan of a single 'cell'. As soon as τ_{cell} attains the value $\tau_{\max}$, the 'cell' undergoes division into two. $\tau_{\max}$ is the parameter of the model.

'Cell' behaviour in the present model is determined by three parameters: (1) cellular motility, i.e. path l travelled by the 'cell' during time τ; (2) chemotactic responsiveness T_1; and (3) chemotactic sensitivity, i.e. the minimum difference between attractant concentrations to which the 'cell' can respond:

$$\min \Delta C_0 = \min[C_0(t+\tau) - C_0(t)] .$$

Fig. 27 demonstrates the formation of stable wave patterns (a–c) and development of instability (d–f) in a computer simulation based on the automaton model described earlier. The initial stages of the two-wave regimes are seen to be very similar in that ring-shaped structureless 'cell' populations resembling those observed in *in vivo* experiments arise and propagate from the origin (Fig. 25). However, subsequent stages are essentially different. The likelihood of wave symmetry bursting (Fig. 27d–f) depends on the above cellular parameters, viz. motility l, chemotactic responsiveness T_1, and chemotactic sensitivity of the 'cells'. For example, distortion of symmetry may result from impaired chemotactic sensitivity (as in the case of the computer simulation shown in Fig. 27).

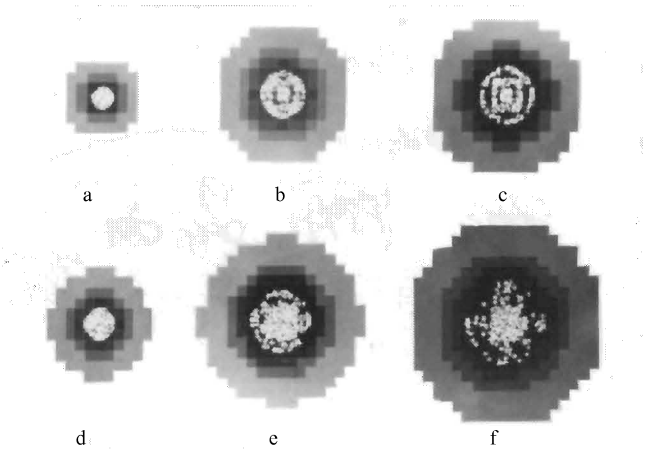

Figure 27. Formation of symmetric (a–c) and asymmetric (d–f) wave patterns in a computer simulation [124]. A stationary (motionless) ring is formed behind the propagating population wave (b). Characteristic parameters: $T_1 = 4$; $l = 0.8$; $\min \Delta C_0 = 1$ (for symmetric wave patterns) and $T_1 = 4$; $l = 0.8$; $\min \Delta C_0 = 10$ (for asymmetric wave patterns).

It follows from Fig. 28 that the parameter space $(l, T_1, \min \Delta C_0)$ is divided into two regions: RW (where regular symmetric wave patterns occur) and DW (where symmetry is distorted). Fig. 28 shows that the transition RW → DW is virtually independent of the chemotactic responsiveness unless motility l exceeds 1. Critical values of chemotactic sensitivity increase dramatically with increasing motility provided the chemotactic response is not abnormally high (Fig. 28).

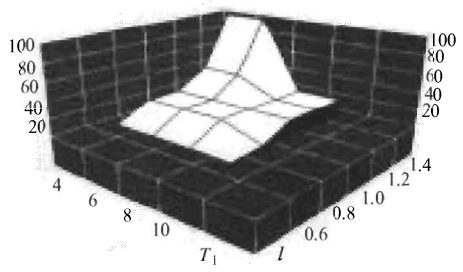

Figure 28. The interface between RW and DW regions in the parameter space (T_1, l, $\min \Delta C_0$). The DW region is located above the interface.

Therefore, this relatively simple mathematical model demonstrates how symmetric autowave patterns formed by motile elements with memory (and chemotaxis) may be distin-guished. It may be suggested that such symmetry bursting is due to fluctuations of bacterial cell density (by analogy with fluctuations in the amoeba *Dictyostelium discoideum* reported to cause instability of cell flow during aggregation [159]).

It follows from Fig. 28 that the transition RW → DW can be obtained in experiments on living cells with reduced motility and cells exhibiting impaired chemotactic sensitivity or strong chemotactic response (provided they retain sufficiently high motility). The former possibility can be easily observed in an experiment (see Fig. 25b). However, it remains to be elucidated whether bacterial density fluctuations are actually responsible for the formation of bursts and, hence, asymmetric wave patterns in *in vivo* experiments, notwithstanding that many authors have provided evidence to confirm the feasibility of such a relationship [91, 123, 159].

Fig. 29 shows a two-dimensional pattern of optical density measured 2 h after the appearance of one of the bursts. Clearly, there is a correlation between its localisation and fluctuations (local rise in bacterial cell density) at the parent population border. It has been shown [123, 159] that such correlation holds for all cases of burst development. However, in certain instances bacterial density fluctuations are not accompanied by the appearance of bursts. One can therefore conclude that fluctuations are necessary but not sufficient to cause symmetry disturbances in bacterial autowave patterns. At the same time, mutations do not appear to constitute a necessary condition for the development of such instabilities. This inference is confirmed by the following evidence [91, 123]. Bacteria from the bursts inoculated into freshly-prepared agar nutrient medium prove to be able to form population waves that propagate at a velocity identical to that of parent population expansion (< 1 mm h^{-1} [91, 123]). These isolates, in turn, give rise to bursts. Results of aminoacid analysis and NMR spectroscopy of samples of medium obtained immediately behind the parent population wave front and just behind the arched boundary of the burst indicate identity of their chemical composition. Moreover, bacteria from bursts and circular

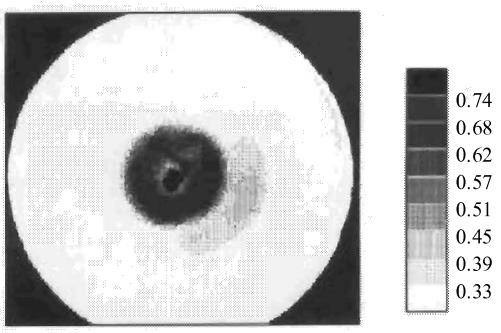

Figure 29. A two-dimensional map showing optical density distribution during burst formation [159]. The scale on the right corresponds to bacterial density. There is a small area of the initial localisation of bacterial cells in the middle of the developing burst.

wave fronts inoculated into fresh nutrient medium have similar doubling time T and exhibit practically identical growth curves ($T \approx 65$ min at 36 °C [91, 123]).

Interestingly, bursts, unlike circular waves [158], are characterised by time-dependent variations of such an important parameter as the average cell length L [91, 123, 158]. Immediately after the bursts appear, their cells are longer (higher values of L) than the cells belonging to the original parent population (Fig. 25b shows such a population as a round spot in the centre of the wave propagation area) (Fig. 30). Cell length distribution maximum at the initial stage of burst formation is shifted towards higher values of L (Fig. 30b) as compared with a similar maximum in the parent cell population (Fig. 30a). Three hours later, both the maximum of cell length distribution and the average cell length return to the initial values characteristic of the parent population (Fig. 30c) [91, 123, 158]. It has been shown that cell redistribution in relation to their length is governed by: (a) a rise in the number of cells when their density decreases and an increase in the cell length with the resulting enhancement of cell density in the population [161], and (b) the relationship between cell motility and length in *E. coli* [162].

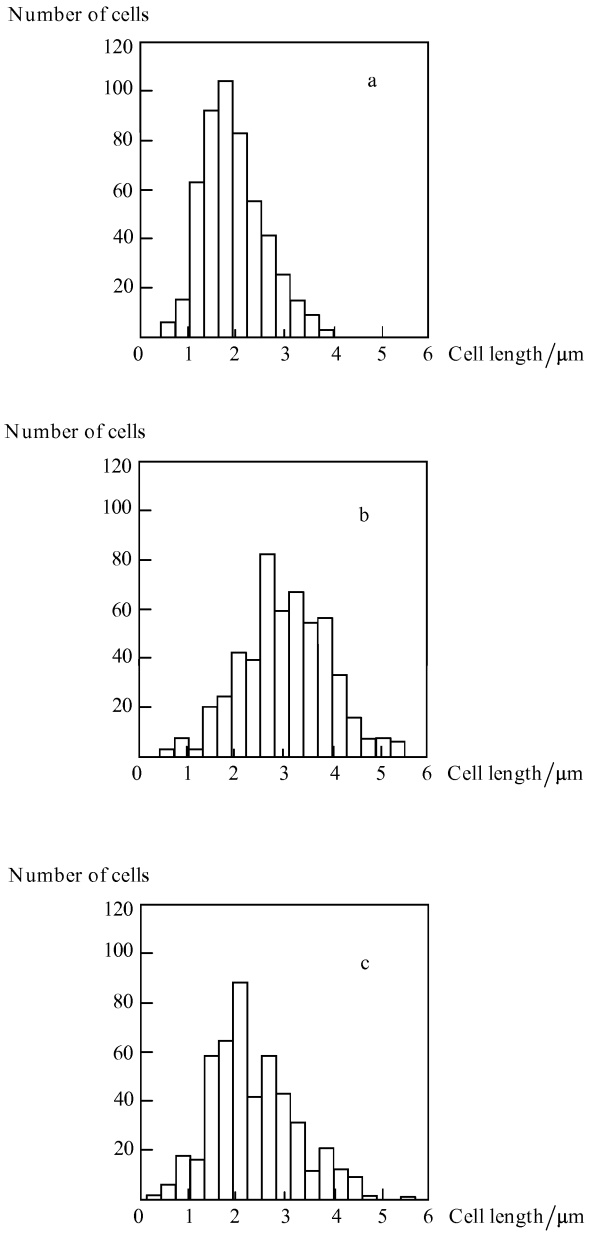

Figure 30 Cell distribution in relation to their length (a) in the parent population and in bursts: (b) immediately after their appearance and (c) 3 hours later [91, 123, 159].

It is noteworthy that bursts failed to develop when the propagation velocity of bacterial population waves was in excess of a critical level U_{cr} approaching 1 mm h^{-1}. Wave velocities $U > U_{cr}$ were reached when agar concentration was reduced to 0.3% or below [91]. Only slow waves proved unstable. Their low velocities were probably due to a relatively high agar concentration. In fact, motile bacteria living in the agar medium collide from time to time with agar fibres and come to a stop [163]. This results in reduced cell motility and wave propagation rate with increasing agar density. These findings suggest that low motility of cells may be responsible for parametric instability of bacterial population waves.

The mechanism of such instability has been explained as follows [91, 123, 159]. Bursts are formed if the most motile and initially few cells travelling ahead of the front formed by the expanding parent population are given sufficient time for their density to increase significantly (as a result of reproduction) and produce their chemotaxis wave before the approaching front takes them up and thus absorbs the developing burst (Fig. 31).

It is appropriate to use model (59), (60) in order to estimate U_{cr}. For bacteria travelling ahead of the parent population front we have [91]:

$$b = \varepsilon\beta\,,$$
$$p = p^* + \varepsilon\pi\,,$$
$$\lambda(p) = \lambda_0\,,$$
$$r(p) = r(p^*) + \varepsilon\pi(p^* + \varepsilon\pi + P_k)\,, \qquad (100)$$

where p^* is a constant, $p^* > p_0$, and ε is a small parameter ($\varepsilon > 0$). Since $\lambda_0 < r(p^*) \sim 1$ [118], substitution of expres-

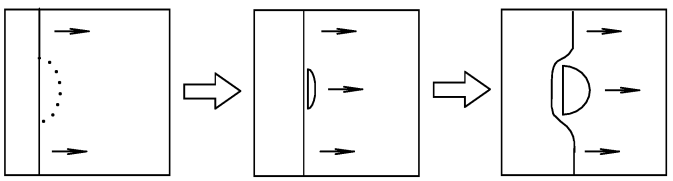

Figure 31. Hypothetical mechanism of bacterial wave instability and burst formation. The dotted line indicates scarcely visible confines of the nascent burst and the edge of the propagating parent population. Arrows show the direction of the wave propagation.

sions (100) into model (59), (60) allows equation (59) to be linearised and represented in the form [91, 123]:

$$\frac{\partial\beta}{\partial t} \cong \beta \,.$$

Hence,

$$t = \ln\frac{\beta}{\beta_0}\,, \tag{101}$$

where $\beta_0 = \beta\,(t=0)$. τ in equation (101) is dimensionless time [118]. Dimensional time is

$$t^* = \frac{1}{K}\,t\,,$$

where $K = 0.76\ \mathrm{h}^{-1}$ [136]. Therefore,

$$t^* = \frac{1}{K}\ln\frac{\beta}{\beta_0}\,. \tag{102}$$

During the time interval t^*, bacterial cell density ahead of the advancing parent population front increases from β_0 to β. The critical velocity is

$$U_{\mathrm{cr}} = \frac{L}{t} = KL\,\ln^{-1}\frac{\beta}{\beta_0}\,, \tag{103}$$

where L is the characteristic size of the developing protuberance. Normally $L \approx 5$ mm [91, 123]. Therefore, at $\beta/\beta_0 \sim 10^2 - 10^3$, $U_{\mathrm{cr}} = 0.6 - 0.8$ mm h^{-1}. This value is in good agreement with experimental results [91, 123, 159].

The mechanism of symmetry bursting of wave patterns formed by chemotactic bacteria has in the main been studied experimentally. Analytic generalisations of the available data have so far not been reported. It is reasonable to assume, however, that the approach employed by Kuramoto in his autowave stability studies [148–151, 153, 154] is equally applicable to investigations of population waves formed by elements with memory (and their mathematical models). Specifically, this approach may prove fruitful not only in studies of the disturbance of the symmetry of wave patterns but also in studies of the mechanisms underlying instability of bacterial population waves. Mathematical models of such waves (see above) being essentially different from the classical model of the 'reaction–diffusion' type (9), (10), it seems safe to prognosticate the discovery of new instability mechanisms.

4.3 Instability of population autowaves generated by chemotactic cells

The previous subsection was dedicated to spontaneous bursting of symmetric autowave patterns developing in a system during its motion in the parameter space. Equally important are the possible mechanisms of instability of population waves formed by chemotactic cells and propagating in real space and time.

Fig. 32a shows a fragment of the population wave front generated by chemotactic amoeba *Dictyostelium discoideum* in the gradient of an attractant (folic acid). Front stability was found to deteriorate with increasing gradient: isolated cell clusters were formed rather than a continuous front and these clusters travelled along the attractant gradient (Fig. 32b). A similar front 'perforation' has been observed in the propagation of population waves formed by chemotactic bacterial cells of *E. coli* (Fig. 33). It can be postulated that in this case the instability is associated with the

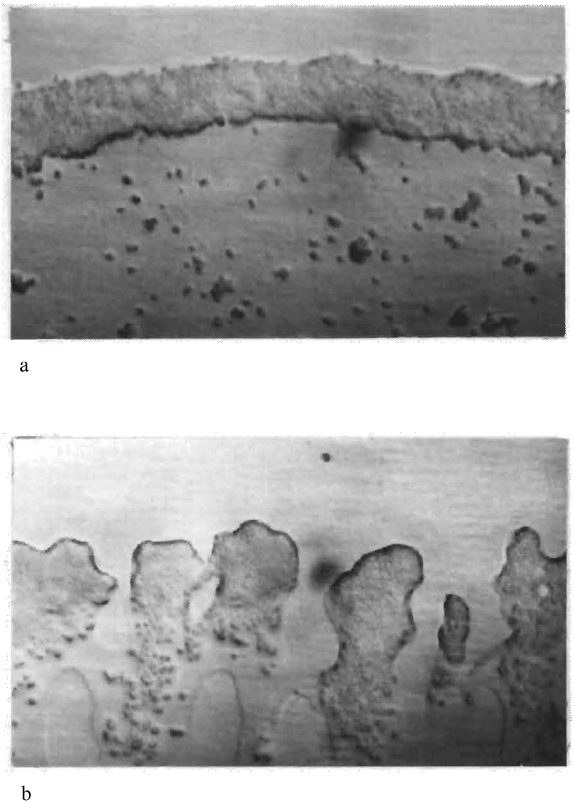

Figure 32. Zones of stable (a) and unstable (b) population waves generated by *Dictyostelium discoideum* cells.

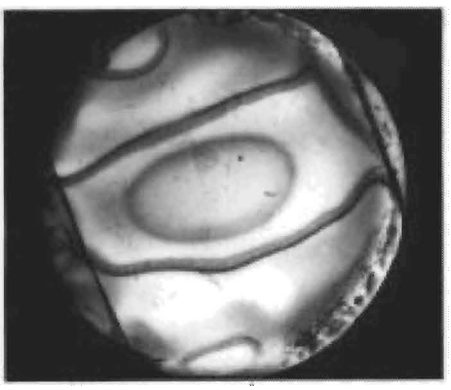

Figure 33. An unstable bacterial population wave [172] with 'perforated' sites.

presence of 'forbidden directions' [156] as follows, for example, from formulae (93), (94). It remains, however, unclear what is the relationship between these mathematical formulae and experimentally observed instabilities of cell population autowaves. Extensive studies of the mechanisms of such instabilities are currently under way.

5. Synopsis

Thus, 'memory' of the medium, i.e. its refractoriness, is responsible for specific wave phenomena in many active media (Table 1). Such specificity has led to the special term 'autowaves' being coined [1, 76, 77, 79].

A separate class of autowaves are waves in active media in which individual elements have memory. Memory

enables these elements to 'trace' changes in the parameters of their environment and 'organise' their own motion taking into account these changes. Therefore, in addition to memory, these elements possess taxis. An example of such 'nonclassical' autowaves is provided by population waves formed by motile chemotactic bacterial cells [13, 91, 93].

Mathematical models of these waves [see for instance equations (24), (25) and (59), (60)] differ from the classical equations of the 'reaction–diffusion' type (9), (10) in that they include terms which describe the directed component of cell motion arising from their chemotactic properties. Equations of this kind need further investigation.

In this context, experimental studies may provide a deeper insight into the role of cellular memory as a factor involved in the formation of spatial structures. It is important to identify effects that are specific to systems generated by particles with memory (and chemotaxis). It is noteworthy that such specificity is lacking in processes giving rise to spatial KΩ-like structures. Indeed, KΩ-like structures have been reported to arise not only upon convergence of bacterial population waves [13, 118, 123, 124, 136, 138, 139] but also when chemical autowaves formed by reagent molecules evidently devoid of memory and chemotaxis approach each other [161]. At the same time, it can be expected that specific memory effects should in the first place manifest themselves in new, nonclassical instability mechanisms operating in spatial structures generated by active media. For example, distortions of the symmetry of autowave patterns generated by motile bacteria and the process of burst development are largely dependent on chemotactic properties, i.e. the memory of individual cells [see formula (5)] [107]. The duration of burst development t^* defined by expression (102) and amounting to a few hours may be regarded as the duration of information memory at the cell population level [73]. It is three orders of magnitude greater than the duration of information memory for an individual bacterial cell [171] as it appears in equation (5).

Investigation of the simplest nonlinear (autowave) systems with memory elements may be of interest not only for the physics of autowaves but also for understanding the mechanisms of thinking. Already a long time ago, it was postulated that in the course of evolution higher organisms came into being from primitive ones by means of association, with the concomitant loss of certain properties and the development of new ones owing to the cooperative effect. Observation of the social life of microorganisms provides striking examples of their metamorphosis. Two fundamental inferences can be deduced from the foregoing discussion, one pertaining to biophysics and the other to the development of new information technologies.

1. The environment for individual cells of a multicellular organism is formed by its internal milieu. In the case of neurons, such milieu is composed of the cerebral fluid and the products of metabolic activity of glial cells and other neurons. Clearly, the behaviour of all cells in the body is totally dependent on the ability of the internal milieu to maintain its properties within physiological limits. Deviation of its parameters beyond the physiological range may have most deleterious effects, regardless of the causative factors [1].

It is possible to distinguish two groups of factors responsible for different forms of collective behaviour of cells. One group depends on environmental parameters, whereas the other is related to the internal, genetically controlled program of organism development which originated in the course of evolution.

In different types of cells, the flexibility of the behaviour program and the possibility of its modification (i.e. learning) vary in a broad range. In this way, the past (the evolutionary history) and the present come together [165].

2. The properties of living cells: memory, taxis, motility, and reproduction, may prove helpful in the development of a new generation of information systems. The first steps in this direction, even if modest, have already been made [166]. Technical implementation of systems with memory, taxis, and motility gave rise to TV automata with tracing scanners. One of such machines was constructed in this Institute as early as in 1970 [167] and later used as a prototype in the commercial production of the "Morphoquant" apparatus for computer identification and analysis of human chromosomes (jointly with Karl Zeiss, Jena).

The advantage of technical implementation of 'cell' behaviour based on such intrinsic properties as memory, taxis, and motility is in saving time as compared with TV automata that analyse visual images line by line. This time saving is approximately equal to the ratio of the total path traversed by the probe during line-by-line scanning to the total perimeter of information zones. This value is normally in the range of 10 to 100, depending on the character of the image, but may significantly increase if 'cells' are capable of reproducing themselves.

The very first attempts to develop artificial reproducing systems date back to the 1950s. One of such algorithms was proposed and realised in 1960 [168]. There are scores of potential modes of using active media for reproducing analytic probes, i.e. 'cells'. Such media include chemically active media supplemented with photosensitive ruthenium-based catalysts, matrices of active (nonlinear) elements and photodiodes arranged in feedback loops, liquid-crystal photosensitive media, spin-glasses, matrices of photosensitive protein molecules (e.g. rhodopsin), and solid-phase photosensitive matrices with combinations of p–n junctions [165]. It remains to be seen which media will find practical application. This is a matter of technological progress and market competition.

Although autowave principles of the analysis of external signals (e.g. images) may be used in brain processes associated with thinking, it is not nearly enough to understand these principles for being able to answer the question that interests us most: how do we think? It can be argued that thinking is essentially cognition and modelling of the environment, the quality of the models being determined by the reaction of the surroundings to their application. L Frobenius, a German ethnographer, maintains that humans construct models of the natural order of things based on the way they apprehend it [169]. This observation was made apropos of religious rites, but it may be equally true as regards the process of cognition and thinking in general. Modelling of the environment appears to be an intrinsic feature of sufficiently complex systems. A major requisite of such modelling is the presence in the system of blocks that are only weakly involved in processing of current information. These blocks analyse different scenarios of the development of a given situation. This mode of model construction is similar to playing a

game [170], and its further exploration may be crucial for better understanding of the phenomenon of thinking. Evaluation of effective data processing algorithms including autowave algorithms is only the first step towards this goal.

Thinking implies the ability to doubt and have compassion, to be inspired and terrified, to estimate possible effects of one's actions. Human brain is the sole highly-organised structure in which these abilities are intrinsic. Neither bacteria nor computers have any of these faculties and seem to be none the worse for that. If, in pursuit of delusive happiness, humans simplify their lives to the extent that they have nothing but instincts to live on, they may be misled by a deceptive feeling of the simplicity of the world and commit many serious mistakes which may threaten their very survival as a biological species.

Acknowledgement. This work was supported in part by Grant RMW000 from the International Science Foundation.

References

1. Ivanitsky G R *Neiroinformatika i Mozg* (Neuroinformatics and Brain) (Moscow: Znanie, 1991)
2. Ashby W R *Design for a Brain* (London: Chapman and Hall, 1960) (Translated into Russian; Moscow: Izd. Inostr. Lit., 1962)
3. Turing A M "Can the machine think? ", in *The World of Mathematics* (Ed. J R Newman) (New York: Simon and Schuster, 1956) Vol. 4, p. 2099 (Translated into Russian; Moscow: Izd. Inostr. Lit., 1960)
4. Searle J R *Sci. Am.* **262** (1) 9 (1990)
5. Godel K *Monatsh. Math. Phys.* **38** 173 (1931)
6. Nagel E, Newman J R *Godel's Proof* (London: Routledge & Kegan Paul, 1958)
7. Kolmogorov A N *Probl. Peredachi Inf.* (1) 3 (1965)
8. Kolmogorov A N *Probl. Peredachi Inf.* (5) 3 (1965)
9. Shuster H G *Deterministic Chaos* (Weinheim: Physik-Verlag, 1984)
10. Kravtsov Yu A *Usp. Fiz. Nauk* **158** 93 (1989) [*Sov. Phys. Usp.* **32** (1989)]
11. Abu-Mostafa Ya S, Psaltis D *Sci. Am.* **256** (3) 66 (1987)
12. Tank D W , Hopfield J J *Sci. Am.* **257** (6) 62 (1987)
13. Ivanitskii G R, Medvinskii A B, Tsyganov M A *Usp. Fiz. Nauk* **161** 13 (1991) [*Sov. Phys. Usp.* **34**(4) 289 (1991)]
14. Cross M *New Sci.* (26 January 1991) 51
15. Cohn F *Beitr. Biol. Pflanz.* **1** 127 (1875)
16. Engelman T W *Pflugers Arch. Gesamte Physiol. Menschen Tiere* **25** 285 (1881)
17. Engelman T W *Pflugers Arch. Gesamte Physiol. Menschen Tiere* **26** 537 (1881)
18. Engelman T W *Pflugers Arch. Gesamte Physiol. Menschen Tiere* **30** 95 (1883)
19. Pfeffer W *Unters. Bot. Inst. Tubingen* **1** 363 (1884)
20. Lengeler J W *La Recherche* **21** 20 (1990)
21. Berg H C *Sci. Am.* **233** (1) 36 (1975)
22. Berg H C *Nature (London)* **254** 389 (1975)
23. Berg H C, Brown D A *Nature (London)* **239** 500 (1972)
24. Macnab R M *Trends Biochem. Sci.* **4** 10 (1979)
25. Adler J *Sci. Am.* **234** (4) 40 (1976)
26. Koshland D E Jr *Physiol. Rev.* **59** 811 (1979)
27. Tsang N, Macnab R M, Koshland D E Jr *Science* **181** 60 (1973)
28. Macnab R M, Koshland D E Jr *Proc. Nat. Acad. Sci. USA* **69** 2509 (1972)
29. Koshland D E Jr *FEBS Lett.* **40** S3 (1974)
30. Glagolev A N *Usp. Mikrobiol.* **18** 163 (1983)
31. Adler J *Science* **166** 1588 (1969)
32. Adler J, Hazelbauer G L, Dahl M M *J. Bacteriol.* **115** 824 (1973)
33. Mesibov R E, Adler J *J. Bacteriol.* **112** 315 (1972)
34. Hazelbauer G L, Mesibov R E, Adler J *Proc. Nat. Acad. Sci.USA* **64** 1300 (1969)
35. Adler J, in *Primitive Sensory and Communication Systems: The Taxes and Tropisms of Micro-Organisms and Cells* (Ed. M J Carlile) (London: Academic Press, 1975) p. 92
36. Tso W-W, Adler J *J. Bacteriol.* **118** 560 (1974)
37. Macnab R M, Koshland D E Jr *J. Mol. Biol.* **84** 399 (1974)
38. Taylor B L, Koshland D E Jr *J. Bacteriol.* **123** 557 (1975)
39. Taylor B L, Miller J B, Warrick H M, Koshland D E Jr *J. Bacteriol.* **140** 567 (1979)
40. Carlile M J, in Ref. [35], p. 1
41. Lenci F, Colombetti G *Ann. Rev. Bioengin.* **7** 341 (1978)
42. Nultsch W, in Ref. [35], p. 30
43. Adler J *J. Gen. Microbiol.* **74** 77 (1973)
44. Imae Y, Mizuno T, Maeda K *J. Bacteriol.* **159** 368 (1984)
45. Imae Y, in *Sensing and Response in Microorganisms* (Eds M Eisenbach, M Balaban) (Amsterdam: Elsevier, 1985) p. 73
46. Ingraham J, in *Escherichia coli and Salmonella typhimorium. Cellular and Molecular Biology* (Ed. F C Neidhardt) (Washington: American Society for Microbiology, 1981) Vol. 1, p. 1543
47. Miller J B, Koshland D E Jr *J. Mol. Biol.* **111** 183 (1977)
48. Frankel R B, Blakemore R P *Bioelectromagnetics* **10** 223 (1989)
49. Eckert R *Science* **176** 473 (1972)
50. Eisenbach M, Zimmerman J R, Ciobotariu A, Fischler H, Korenstein R *Bioelectrochem. Bioenerg.* **10** 499 (1983)
51. Plesset M S, Whipple C G, Winet H *J. Theor. Biol.* **59** 331 (1976)
52. Plesset M S, Winet H *Nature (London)* **248** 441 (1974)
53. Kessler J O *Comm. Theor. Biol.* **1** 85 (1989)
54. Kessler J O *Nature (London)* **313** 218 (1985)
55. Kessler J O *J. Fluid Mech.* **173** 191 (1986)
56. Kessler J O *Contemp. Phys.* **26** 147 (1985)
57. Macnab R M, in Ref. [46], p. 732
58. Taylor B L, Koshland D E Jr *J. Supramol. Struct.* **4** 343 (1976)
59. Poglazov B F, Metlina F L, Novikov V V *Izv. Akad. Nauk SSSR Ser. Biol.* (5) 672 (1981)
60. Berg H C *Ann. Rev. Biophys. Bioengin.* **4** 119 (1975)
61. Adler J *J. Supramol. Struct.* **4** 305 (1976)
62. Russo A F, Koshland D E Jr *Science* **220** 1016 (1983)
63. Russo A F, Koshland D E Jr, in Ref. [45], p. 27
64. Strange P G, Koshland D E Jr *Proc. Nat. Acad. Sci. USA* **73** 762 (1976)
65. Zukin R S, Koshland D E, Jr *Science* **193** 405 (1976)
66. Zukin R S *Biochemistry* **18** 2139 (1979)
67. Dahlquist F W, Elwell R A, Lovely P S *J. Supramol. Struct.* **4** 329 (1976)
68. Brown D A, Berg H C *Proc. Nat. Acad. Sci. USA* **71** 1388 (1974)
69. Block S M, Segall J E, Berg H C *J. Bacteriol.* **154** 312 (1983)
70. Delbruck M, Reichardt W, in *Cellular Mechanisms in Differentiation and Growth* (Ed. D Rudnick) (Princeton, NJ: Princeton University Press, 1956) p. 3
71. Manson M D *Adv. Microb. Physiol.* **33** 277 (1992)
72. Springer M S, Goy M F, Adler J *Nature (London)* **280** 279 (1979)
73. Crutchfield J P, Packard N H *Int. J. Theor. Phys.* **21** 433 (1982)
74. Ivanitskii G R *Nauka i Chelovechestvo* (Science and Mankind) (Moscow: Znanie,1982) p. 211
75. Ivanitsky G R, Krinsky V I, Zaikin A N, Zhabotinsky A M *Sov. Sci. Rev. D* **2** 279 (1981)
76. Krinskii V I, Zhabotinskii A M *Avtovolnovye Protsessy v Sistemakh s Diffuziei* (Autowave Processes in Systems with Diffusion) (Ed. M T Grekhova, V A Antonets, V I Krinskii, L A Ostrovskii, M I Rabinovich, V G Yakhno) (Gorky: Inst. Appl. Phys. Acad. Sci. USSR, 1981) p. 6

77. Romanovskii Yu M , Stepanov N V, Chernavskii D S *Matematicheskaya Biofizika* (Mathematical Biophysics) (Moscow: Nauka, 1984)
78. Kolmogorov A N, Petrovskii I E, Piskunov N S *Vopr. Kibern.* (12) 3 (1975)
79. Krinskii V I, Medvinskii A B, Panfilov A V *Evolyutsiya Avtovolnovykh Vikhrei (Volny v Serdtse)* [Evolution of Autowave Vortices (Waves in the Heart)] (Moscow: Znanie, 1986)
80. Franck U F, in *Biological and Biochemical Oscillators* (Eds B Chance, E K Pye, A K Ghosh, B Hess) (New York: Academic Press, 1973) p. 7
81. Kerner B S, Osipov V V *Usp. Fiz. Nauk* **160** (9) 1 (1990) [*Sov. Phys. Usp.* **33** 679 (1990)]
82. Kerner B S, Krinskii V I, Osipov V V, in *Thermodynamics and Pattern Formation in Biology* (Berlin: De Gruyter, 1988) p. 265
83. Gierer A, Meinhardt H *Kybernetics* **12** 30 (1972)
84. Meinhardt H, Gierer A *J. Cell Sci.* **15** 321 (1974)
85. Meinhardt H *J. Cell Sci.* **23** 117 (1977)
86. Gierer A *Naturwissenschaften* **68** 245 (1981)
87. Nicolis G, Prigogine I *Self-Organization in Non-equilibrium Systems* (New York: Wiley, 1977)
88. Nagumo J, Yoshizawa S, Arimoto S *IEEE Trans. Commun. Technol.* **12** 400 (1965)
89. Khramov R N *Biofizika* **23** 871 (1978)
90. Khramov R N, Krinskii V I *Biofizika* **22** 512 (1978)
91. Medvinskii A B, Tsyganov M A, Kutyshenko V P, Shakhbazyan V Yu, Kresteva I B, Kuzmin S V, Lisanskaya V Ya, Ivanitskii G R, *Dokl. Akad. Nauk SSSR* **323** 236 (1993)
92. Adler J *J. Bacteriol.* **92** 121 (1966)
93. Adler J *Science* **153** 708 (1966)
94. Adler J, Dahl M M *J. Gen. Microbiol.* **46** 161 (1967)
95. Adler J, Templeton B *J. Gen. Microbiol.* **46** 175 (1967)
96. Keller E F, Segel L A *J. Theor. Biol.* **30** 225 (1971)
97. Keller E F, Segel L A *J. Theor. Biol.* **30** 235 (1971)
98. Chandrasekhar S *Rev. Mod. Phys.* **15** 57 (1943)
99. Keller E F, Segel L A *J. Theor. Biol.* **26** 399 (1970)
100. Dalquist F W, Lovely P, Koshland D E Jr *Nature (London) New Biol.* **236** 120 (1972)
101. Scribner T L, Segel L A, Rogers E H *J. Theor. Biol.* **46** 189 (1974)
102. Lapidus I R, Schiller R *Biophys. J.* **16** 779 (1976)
103. Mesibov R, Ordal G W, Adler J *J. Gen. Physiol.* **62** 203 (1973)
104. Clarke S, Koshland D E Jr *J. Biol. Chem.* **254** 9695 (1979)
105. Segel L A, in *Physical and Chemical Aspects of Cell Surface Events in Cellular Regulation* (Eds C De Lisi, R Blumenthal) (New York: Elsevier, 1979) p. 293
106. Boon J-P, Herpigny B *Bull. Math. Biol.* **48** 1 (1986)
107. Zavalskii L Yu, Svetogorov D E, Brezgunov V N, Popov V G *Dokl. Akad. Nauk SSSR* **279** 488 (1984)
108. Zavalskii L Yu, Svetogorov D E, Brezgunov V N *Biofizika* **30** 93 (1985)
109. Zavalskii L Yu *Biofizika* **33** 328 (1988)
110. Rivero M A, Tranquillo R T, Buettner H M, Lauffenburger D A *Chem. Eng. Sci.* **44** 2881 (1989)
111. Segel L A *SIAM J. Appl. Math.* **32** 653 (1977)
112. Nossal R, Chen S H *Nature (London) New Biol.* **244** 253 (1973)
113. Alt W *J. Math. Biol.* **9** 147 (1980)
114. Ford R M, Lauffenburger D A *Bull. Math. Biol.* **53** 721 (1991)
115. Macnab R M, in *Biological Regulation and Development* (Ed. R Goldberger) (New York: Plenum Press, 1980) p. 377
116. Ford R M, Quinn J A, Phillips B R, Lauffenburger D A *Biotechnol. Bioeng.* **37** 647 (1991)
117. Ford R M, Lauffenburger D A *Biotechnol. Bioeng.* **37** 661 (1991)
118. Medvinsky A B, Tsyganov M A, Shakhbazian V Yu, Kresteva I B, Ivanitsky G R *Physica D* **64** 267 (1993)
119. Budrene E O *Dokl. Akad. Nauk SSSR* **283** 470 (1985)
120. Budrene E O *Biofizika* **33** 373 (1988)
121. Ivanitskii G R, Krinskii V I, Tsyganov M A, Agladze K I *Biofizika* **33** 372 (1988)
122. Agladze K I, Budrene E, Ivanitsky G R, Krinsky V I, Tsyganov M A, Shakhbazian V Yu *Proc. Roy. Soc. London B* **253** 131 (1993)
123. Medvinskii A B, Doctoral Thesis Phys.-Math. Sciences (Pushchino: Inst. Theor. Exptl. Biophys., 1993)
124. Tsyganov M A, Medvinskii A B, Ponomareva V M, Ivanitskii G R *Dokl. Akad. Nauk SSSR* **306** 731 (1989)
125. Shakhbazyan V Yu, Medvinskii A B, Agladze K I, Tsyganov M A, Ivanitskii G R *Dokl. Akad. Nauk SSSR* **310** 737 (1990)
126. Reshetilov A N, Medvinskii A B, Eliseeva T R, Shakhbazyan V Yu, Tsyganov M A, Boronin A M, Ivanitskii G R *Dokl. Akad. Nauk SSSR* **323** 971 (1992)
127. Reshetilov A N, Medvinsky A B, Eliseeva T P, Shakhbazian V Yu, Boronin A M, Ivanitsky G R *FEMS Microbiol. Lett.* **94** 59 (1992)
128. Holz M, Chen S-H *Biophys. J.* **26** 243 (1979)
129. Zhabotinskii A M *Kontsentratsionnye Avtokolebaniya* (Concentration Autooscillations) (Moscow: Nauka, 1974)
130. Krinskii V I, Mikhailov A S *Avtovolny* (Autowaves) (Moscow: Znanie,1984)
131. Vol'kenstein M V *Biofizika* (Biophysics) (Moscow: Nauka,1981)
132. Winfree A T *The Geometry of Biological Time* (Berlin: Springer, 1980)
133. Winfree A T *When Time Breaks Down. The Three-Dimensional Dynamics of Electrochemical Waves and Cardiac Arrhythmias* (Princeton, NJ: Princeton University Press, 1987)
134. Vasilev V A, Romanovskii Yu M, Chernavskii D S, Yakhno V G *Autowave Processes in Kinetic Systems* (Dordrecht, Holland: Kluwer, 1987)
135. Kerner B S, Osipov V V *Usp. Fiz. Nauk* **157** 201 (1989) [*Sov. Phys. Usp.* **32** 101 (1989)]
136. Medvinsky A B, Shakhbazian V Yu, Tsyganov M A, Ivanitsky G R *FEMS Microbiol. Lett.* **84** 279 (1991)
137. Lauffenburger D, Kennedy C R, Aris R *Bull. Math. Biol.* **46** 19 (1984)
138. Medvinskii A B, Shakhbazyan V Yu, Tsyganov M A, Baryshnikova L M, Ivanitskii G R *Dokl. Akad. Nauk SSSR* **317** 1001 (1991)
139. Tsyganov M A, Kresteva I B, Medvinskii A B, Ivanitskii G R *Dokl. Akad. Nauk SSSR* **333** 532 (1993)
140. Belintsev B J, Belousov L V, Zaraisky A G *J. Theor. Biol.* **129** 369 (1987)
141. Busa W B, Nuccitelli R *J. Cell. Biol.* **100** 1324 (1985)
142. Robertson A D, Grutsch J F *Cell.* **24** 603 (1981)
143. Siegert F, Weijer C J *Physica D* **49** 224 (1991)
144. Steinbock O, Hashimoto H, Muller S C *Physica D* **49** 223 (1991)
145. Turing A M *Phil. Trans. Roy. Soc. London B* **237** 37 (1952)
146. Kokochashvili V I, Candidate Thesis, Phys-Math. Sciences (Moscow: Inst. Chem. Phys. Acad. Sci. USSR, Tbilisi Univ., 1942)
147. Zeldovich Ya B *Teoriya Goreniya i Detonatsii Gazov* (The Theory of Combustion and Detonation of Gases) (Moscow: Izd. Akad. Nauk SSSR, 1944)
148. Kuramoto Y, Yamada T *Prog. Theor. Phys.* **55** 679 (1976)
149. Kuramoto Y *Prog. Theor. Phys.* **63** 1885 (1980)
150. Kuramoto Y, Koga S *Phys. Lett. A* **92** 1 (1982)
151. Kuramoto Y *Chemical Oscillations, Waves, and Turbulence* (Berlin: Springer, 1984)
152. *Kolebaniya i Begushchie Volny v Khimicheskikh Sistemakh* (Oscillations and Travelling Waves in Chemical Systems) (Translated into Russian; Moscow: Mir, 1988)
153. Yamada T, Kuramoto Y *Prog. Theor. Phys.* **56** 681 (1976)
154. Kuramoto Y *Prog. Theor. Phys. Suppl.* **64** 346 (1978)
155. Kerner B S, Osipov V V *Avtosolitony* (Autosolitons) (Moscow: Nauka, 1991)
156. Mornev O A, Candidate Thesis, Phys-Math. Sciences (Pushchino: Inst. Biol. Phys. Acad. Sci. USSR, 1989)
157. Merkin V S, Pastushenko V F, Chizmadzhev Yu A *Teoriya Vozbudimykh Sred* (The Theory of Excitable Media) (Moscow: Nauka, 1981)

158. Medvinskii A B, Fishov I L, Tsyganov M A, Ivanitskii G R *Dokl. Akad. Nauk* **311** 1479 (1990)
159. Medvinsky A B, Tsyganov M A, Kutyshenko V P, Shakhbazian V Yu, Kresteva I B, Ivanitsky G R *FEMS Microbiol. Lett.* **112** 287 (1993)
160. Levine H, Reynolds W *Phys. Rev. Lett.* **66** 2400 (1991)
161. Medvinskii A B, Shakhbazyan V Yu, Kresteva I B, Tsyganov M A, Kuzmin S V, Ivanitskii G R *Dokl. Akad. Nauk SSSR* **326** 194 (1992)
162. Medvinskii A B, Fishov I L, Karpov V A, Tsyganov M A, Milonova I N, Ivanitskii G R *Dokl. Akad. Nauk SSSR* **318** 454 (1991)
163. Wolf A J, Berg H C *Proc. Nat. Acad. Sci. USA* **86** 6973 (1989)
164. Lee K J, McCormick W D, Quyang Q, Swinney H L *Science* **261** 192 (1993)
165. Ivanitskii G R *Mir Glazami Biofizika* (The World in the Eyes of a Biophysicist) (Moscow: Pedagogika, 1985)
166. Ivanitskii G R (Ed.) *Biotekhnika — Novoe Napravlenie Komp'yuterizatsii* (Biotechnics — a Novel Strategy of Computerisation) (Moscow: Nauka, 1990)
167. Agadzhanian D, Ivanitsky G, Shamarov A ''Scanning method and a scan microscope for its realization'', US Pat. 3 780 298 (1973)
168. Lee C Y *IRE Trans. Elec. Comput.* **EC-10** 346 (1961)
169. Frobenius L *Kulturgeschichte Afrikas. Prolegomena zu einer historischen Gestaltlehre* (Phaidon-Verlag, 1933)
170. Huizinga Y *Homo Ludens in Deschaduwen van Morgen* (Haarlem, 1938) (Translated into Russian; Moscow: Progress; Academia, 1992)
171. Morimoto B H, Koshland D E Jr *FASEB J.* **5** 2061 (1991)
172. Tsyganov M A, Kresteva I B, Medvinskii A B, Ivanitskii G R *Dokl. Ross. Akad. Nauk.* in press